High-entropy alloys

Easo P. George,[1,2] *Dierk Raabe*,[3] *Robert O. Ritchie*[4,5]

[1]Oak Ridge National Laboratory, Materials Science and Technology Division, Oak Ridge Tennessee 37831-6115, USA

[2]University of Tennessee, Department of Materials Science and Engineering, Knoxville, Tennessee 37996-2100, USA

[3]Max-Planck-Institut für Eisenforschung, Department of Microstructure Physics and Alloy Design, 40237 Düsseldorf, Germany

[4]Lawrence Berkeley National Laboratory, Materials Sciences Division, Berkeley, California 94720, USA

[5]University of California, Department of Materials Science & Engineering, Berkeley, California, 94720, USA

Email: georgeep@ornl.gov; egeorge@utk.edu ORCID: 0000-0001-9898-9694

Abstract | Alloying has long been used to confer desirable properties on materials. Typically, it involves the addition of relatively small amounts of secondary elements to a primary element. For about the last decade and a half, however, a new alloying strategy has been in vogue that involves the combination of multiple principal elements in high concentrations to create novel materials called high-entropy alloys (HEAs). The multidimensional compositional space that can be tackled with this approach is practically limitless and only tiny regions have been investigated so far. Nevertheless, a few HEAs have already been shown to possess exceptional properties, exceeding those of conventional alloys, which offers the promise of discovering other outstanding HEAs in the future. Here we review recent progress in understanding the salient features of HEAs. Model alloys whose behavior has been carefully investigated are highlighted and their fundamental properties and responsible elementary mechanisms discussed. We also address the vast compositional space that remains to be explored and outline fruitful ways to identify regions within this space where HEAs with potentially interesting properties may be lurking.

Since the Bronze Age, humans have been altering the properties of materials by adding alloying elements. For example, a few percent by weight of Cu was being added to Ag to produce sterling silver for coinage a thousand years ago because pure silver was too soft. Examples from the modern era include steels that consist primarily of Fe to which elements such as C and Cr are added for strength and corrosion resistance, respectively, and Si doped with parts per million levels of P or B to create *n*-type or *p*-type semiconductors. With few exceptions, the basic alloying strategy of adding relatively small amounts of *secondary elements* to a *primary element* has remained unchanged over millennia. It is even reflected in how alloys are named after their principal constituent: ferrous alloys, Al alloys, Ti alloys, Ni alloys, Cu alloys, *etc*. However, such a "primary-element" approach drastically limits the total number of possible element combinations and, therefore, alloys, most of which have been identified and the useful ones exploited. New approaches are needed if the compositional space for exploration is to be significantly enlarged.

One such approach is based on mixing together *multiple principal elements* in relatively high (often equiatomic) concentrations. It stands in sharp contrast to what has been the traditional practice and has therefore attracted the attention of scientists worldwide. The related surge in research activity, especially during the last five years, can be traced back to the publication of two seminal papers in 2004 [Yeh2004, Cantor2004]. These two groups independently proposed the study of a new class of alloys containing multiple elements in near-equiatomic concentrations. It was subsequently pointed out that conventional alloys tend to cluster around the corners or edges of phase diagrams, where the number of possible element combinations is limited, and that vastly more combinations are available near the centers of phase diagrams, especially in quaternary, quinary and higher-order systems [Cantor2014]. Because of their sheer numbers, little is known about concentrated, multi-component alloys but, by the same token, because there are so many possible combinations, the concept offers promise that interesting new alloys with useful properties will be discovered in their midst.

Yeh *et al*. [2004] provided an additional, intriguing, rationale for investigating these alloys: they hypothesized that the presence of multiple (five or more) elements in near-equiatomic proportions would increase the configurational entropy of mixing by an amount sufficient to overcome the enthalpies of compound formation, thereby deterring the formation of potentially harmful intermetallics. This was a counter-intuitive notion because the conventional

view — likely based on binary phase diagrams where solid solutions are typically found at the ends and compounds near the centers — was that the greater the number of elements in concentrated alloys, the higher the probability that some of the elements will react to form compounds. But Yeh *et al*. reasoned that, as the number of elements in an alloy increased, the entropic contribution to the total free energy would be able to overcome the enthalpic contribution and thereby stabilize solid solutions [for additional details, see **Box 1**]. They coined a catchy new name, *high-entropy alloys*, for this class of materials containing five of more elements in relatively high concentrations (5-35 at.%). Others have suggested alternative names, such as multi-component alloys, compositionally complex alloys and multi-principal-element alloys. However, judging by its popularity in the literature, we suspect that despite entropy not being the prime factor responsible for the structure and properties of these alloys, the term "high-entropy alloys" is likely to be the name that endures.

Box 1: Thermodynamics of phase stability

Consider an alloy created by combining two pure elements A and B. It can form a solid solution or one or more intermetallic phases depending on the relative free energies of the following reactions:

$$\text{A + B = } \underline{\text{AB}} \text{ (solution): } \Delta G_{mix} = \Delta H_{mix} - T\Delta S_{mix} \quad (1)$$

$$\text{A + B = AB (intermetallic): } \Delta G_f = \Delta H_f - T\Delta S_f \quad (2),$$

where ΔG_{mix}, ΔH_{mix}, ΔS_{mix} are, respectively, the Gibbs free energy, enthalpy, and entropy of mixing; ΔG_f, ΔH_f, ΔS_f are corresponding values for the formation of an intermetallic compound with AB stoichiometry; and T is the absolute temperature. If, instead, two intermetallic compounds with different stoichiometries form (AB_2, A_2B, *etc*.), additional expressions similar to Eq. 2 would be needed for each such compound.

At thermodynamic equilibrium, the phases present in the alloy depend on whether the Gibbs free energy of mixing (Eq. 1) is more or less negative than the free energies of formation (Eq. 2) of *all* possible intermetallic compounds comprising the elements A and B (i.e., A_iB_j where $i, j = 1, 2, 3\ldots$) present individually or as mixtures. Note that it is not necessary for A + B to transform *entirely* into A_iB_j type intermetallics; rather, intermetallics can precipitate within an A-rich or B-rich

(terminal) solid solution. In the latter case the relevant free energy change involves the sum of the free energy of mixing of the terminal solid solution and the free energy of formation of the intermetallic. Additionally, if intermetallic compounds are not favored, and only a solid solution forms, the latter need not be random (or ideal) because the different atomic species can cluster or order on the lattice depending on whether the ΔH_{mix} term in Eq. 1 is positive or negative, respectively. Another possibility is that, instead of forming a *single* solid solution, the mixture decomposes into two solid solutions (with different compositions, crystal structures and/or lattice parameters).

The situation becomes increasingly more complex as more and more alloying elements are added (A + B + C + D +…) because the number of possible phases that can co-exist correspondingly increases – as given by the Gibbs phase rule. If some of those phases are intermetallic compounds, they can be of several different types as outlined earlier, even if we consider just the binary pairs (A-B, B-C, A-C, A-D, B-D, C-D, etc.). In reality, ternary and higher-order intermetallics, which need not all be line compounds, can also form, thereby rapidly escalating the number of possibilities. In cases where the compounds exhibit a compositional range of stability, the energies of the defects needed to accommodate deviations from stoichiometry (e.g., anti-site defects) have to be accounted for. Some of the possible mixing reactions are shown schematically in Fig. 1.

Even in simple A-B type alloys, it is rarely the case that there is complete miscibility across the entire composition range (*i.e.*, from pure A all the way to pure B). Rather, binary phase diagrams typically exhibit solid solutions near the pure-element ends and a variety of intermetallic compounds in between, many of which are brittle. The problem is exacerbated in multi-element alloys where, as discussed above, there are many more element pairs that can attract each other and, therefore, an increased number of potentially stable intermetallics (*i.e.*, decreased likelihood of single-phase solid solution formation).

The traditional reluctance of metallurgists to work with concentrated multi-element alloys was turned on its head by Yeh *et al.* [2004] who proposed that the increased configurational entropy of mixing in alloys comprising multiple alloying elements (Eq. 1) would counteract the tendency for compound formation (Eq. 2). In other words, they proposed what was then a radical and counterintuitive idea: by

adding more and more elements at near-equiatomic concentrations, it would be possible to stabilize solid solutions at the expense of intermetallics.

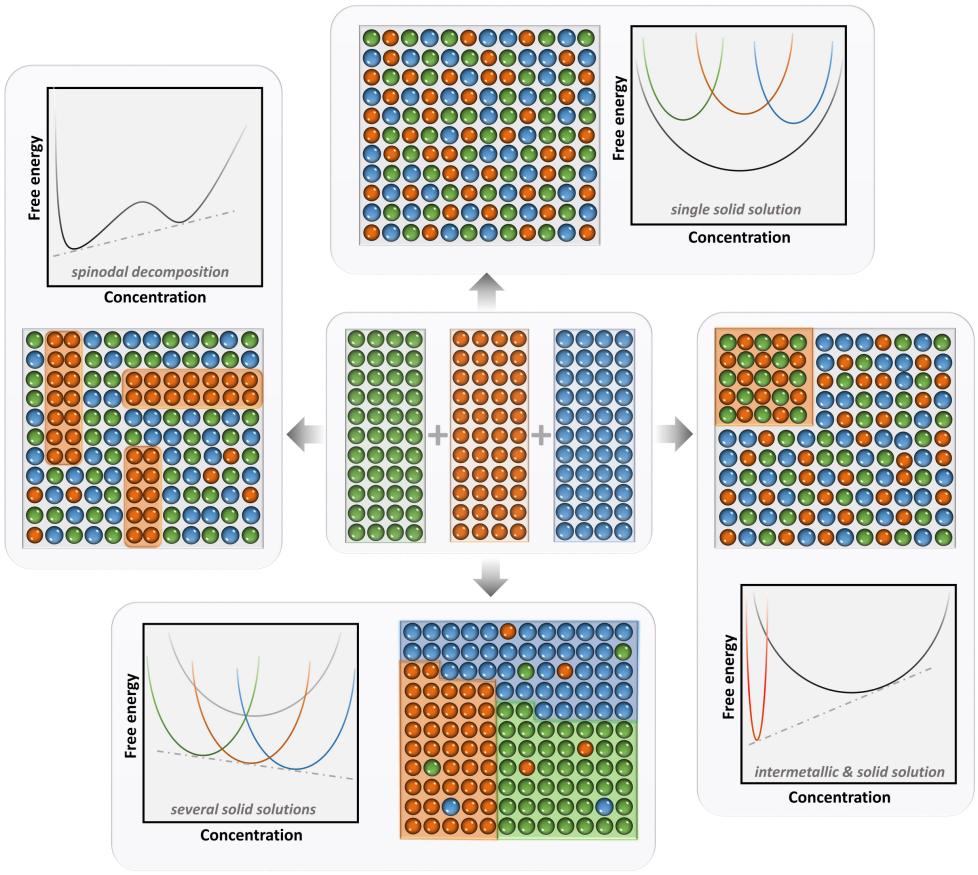

Fig. 1: Some of the possible reactions that can occur when three different elements, represented by the red, blue and green spheres, are mixed in equal proportions (center), including spinodal decomposition (left), formation of single/multiple solid solutions (top/bottom), or precipitation of an intermetallic compound in a solid solution (right).

To make their case, Yeh *et al*. [2004] simplified the problem as follows. They assumed on the one hand that the considered solid solution is ideal, in which case the enthalpy of mixing (ΔH_{mix}) in Eq. 1 is zero and, on the other hand, that the competing intermetallic compound is perfectly ordered, in which case its formation (configurational) entropy (ΔS_{f}) in Eq. 2 is zero. The relative stabilities of the solid

solution and intermetallic compound would then depend on whether $-T\Delta S_{mix}$ (Eq. 1) is more negative than ΔH_f (Eq. 2). The ideal entropy of mixing is given by:

$$\Delta S_{mix} = -R\Sigma x_i \ln x_i \quad (3),$$

where R is the gas constant and x_i is the mole fraction of the i^{th} element. In an equiatomic alloy, $x_1 = x_2 = x_3$, etc. and the mixing entropy becomes:

$$\Delta S_{mix} = R\ln n \quad (4),$$

where n is the number of elements in the alloy, yielding values for ΔS_{mix} of $1.39R$, $1.61R$ and $1.79R$ for equiatomic alloys containing 4, 5 and 6 elements, respectively.

Based on the above simplification, Yeh *et al.* argued that in "alloys with a high number of principal elements" (say, $n = 5$) the entropic contribution to the free energy ($-T_m\Delta S_{mix}$) at the melting temperature T_m is comparable to the formation enthalpies (ΔH_f) of strong intermetallic compounds such as NiAl and TiAl. Therefore, they concluded that high configurational entropy would suppress compound formation "except for those with large heats of formation, such as strong ceramic compounds: oxides, carbides, nitrides, and silicides" thereby "more easily yield(ing) … random solid solutions during solidification". Consequently, they defined high-entropy alloys as those with five of more elements ($n \geq 5$) in equiatomic concentrations. To allow for flexibility in alloy design, they relaxed the equiatomic requirement and permitted a range of concentrations from 5 to 35 at.% for each constituent element. As it turns out, and as discussed in the accompanying text, their simple criterion based on the number of alloying elements is not sufficient to predict single-phase solid solution formation in multi-element alloys.

Interestingly, most of the investigated high-entropy alloys in the early years were multi-phase alloys rather than single-phase solid solutions [e.g., Huang2004, Tong2005, Zhou2007, Wang2008, Shun2010, Singh2011]. In recent years though, increased attention is being paid to a few model single-phase alloys to probe their behavior in greater detail and uncover fundamental mechanisms without the confounding effects of second phases. Investigation of single-phase alloys allows variables such as the number, types and concentrations of alloying elements to be systematically varied and directly correlated with physical and mechanical properties such as elastic constants, stacking fault energies, diffusion coefficients, strength, ductility, *etc*. Such

studies, although important in their own right, have broader applicability also to the understanding of certain multi-phase alloys, such as the advanced γ-γ′ Ni-base superalloys used in jet engines and power generation, in which the matrix phase (γ) is a complex solid solution consisting of multiple elements in relatively high concentrations with none of them being the majority element [Yardley2016]. At least some of the rate-controlling mechanisms that govern the overall properties of the γ-γ′ composite (*e.g.*, dislocation climb) occur within the γ phase or at the γ-γ′ phase boundaries. Thus, a fundamental understanding of the energetics and kinetics of point defects, dislocations and diffusion in complex solid solutions is relevant also to understanding the behavior of multi-phase alloys. Finally, complex solid solutions are important from a basic scientific viewpoint because of the conceptual advances needed to bridge the gap between the relatively well understood dilute solid solutions and poorly understood concentrated solid solutions.

In this review we present some approaches for efficiently probing the huge compositional space of HEAs for desirable structures and mechanisms that can help identify novel materials with interesting features. We first briefly reflect on some HEA success stories – there are not too many to date – using them as examples for discussing pertinent development strategies. Then, we discuss several specific pathways for the identification of new HEAs, namely, a thermodynamic one based on phase diagram calculations [Zhang JOM2012, Zhang2014, Gao2017, Mao2017, Gorsse2018a, Gorsse2018b, Abu-Odeh2018, Chen2018], an experimental combinatorial one [Borkar, 2016, Borkar2017, Kauffmann2017, Li2018c, Li2018d], and a mechanistic one that aims at compositionally tailoring and combining specific microstructure mechanisms such as twinning-induced plasticity (TWIP) [Otto 2013b, Deng Acta2015, Li JOM2017, Jo2017] and transformation-induced plasticity (TRIP) [Li Nature2016, Li Acta2017, Huang2017]. We conclude by discussing prospects and future opportunities for the field, highlighting theoretical and experimental tools that should be developed to identify new HEAs and the directions that should be the focus of future research, including developing HEAs that work well at high temperature and HEAs that display combinations of properties and functionalities that are not found in existing materials.

Single-phase high-entropy alloys

Phase stability and configurational entropy. The appeal of the entropy hypothesis [Yeh2004] lay in its straightforward testable prediction: alloys comprising five or more elements would form single phase solid solutions. However, when put to the test [Otto2013a], it turned out that in several nominally similar five-element alloys, all of them except for one contained

multiple intermetallic phases, showing that configurational entropy is not a useful predictor of which alloys are simple solid solutions. In addition to configurational entropy, one needs to take into account other entropic contributions as well as mixing enthalpies [Otto2013a, Poletti2014, MaActa2015a, Schön2018]. A further complication was that Yeh *et al*.'s analysis was performed at the melting point whereas most alloy microstructures tend to be examined at room temperature. Depending on the diffusion rates, phase transformation kinetics, and cooling rates, room- and high-temperature microstructures may be quite different. Indeed, HEAs often contain multiple phases when examined at room temperature, and many of the second phases are intermetallics that can be brittle and hinder mechanical performance. If the goal is to avoid the formation of such phases, simply mixing together five or more elements in near-equiatomic concentrations is unlikely to be a useful approach. Even multi-component alloys that are initially single phase after solidification tend to separate into multiple metallic and intermetallic phases when annealed at intermediate temperatures [Schuh2015, Pickering2016a, Otto2016, Schuh2018, Stepanov2018]. This phase instability has only recently been recognized as a common feature of many (perhaps most) HEAs and needs to be accounted for when considering alloys for high-temperature applications.

Because phase relationships are governed by the total free energy, the original high-entropy criterion could conceivably be supplemented with a "low-enthalpy" criterion for solid solution stability. In fact, there are many alloys containing fewer than five elements (medium-entropy alloys) that are single-phase solid solutions; these alloys may well be enthalpy-stabilized rather than entropy-stabilized. This relaxes the original high-entropy criterion that alloys should contain five or more elements in near-equiatomic ratios. It also provides a wider composition space for investigation that includes alloys with fewer elements, as well alloys deviating from equiatomic compositions [Ma 2015b, Li2017]. However, determining the enthalpy is not as easy as estimating the configurational entropy of an ideal solid solution. Therefore, although one could christen these alloys as "low-enthalpy alloys," it is less useful as a classification scheme.

Given the importance of predicting and understanding the microstructures of HEAs, several studies have attempted to treat the thermodynamics of phase stability in complex alloys more fully, with varying degrees of success. Truly *ab initio* calculations are tedious, especially at finite temperatures [Tian2013, Ma2015, Van de Walle2002]. Thus, they are probably best suited to screening narrow composition ranges that have already been identified as being of interest (based on other considerations) and when phase stabilities need to be predicted accurately.

Calculations of phase diagrams (CALPHAD)-type approaches, which use software to calculate phase diagrams based on thermodynamic models, in general have broader applicability and have been shown to be useful in predicting phase stability in some cases.

Numerous other studies, summarized elsewhere [Yeh2013, Tsai2014, Zhang2014, Miracle2017], have attempted to relate phase stability to parameters such as size misfits, valence electron concentrations, electronegativities, and mixing enthalpies. However, many of those treatments ignore the formation enthalpies of competing compounds, typically intermetallic phases, which in our view limits their applicability. The typical procedure is to construct empirical "phase stability maps" as functions of the above parameters. "Critical" values for the parameters are then estimated above or below which certain types of microstructures (*e.g.*, solid solutions) are stable. These values appear to be arbitrary and based on back-tested correlations with little evidence of predictive capability. Other, thermodynamically more consistent approaches [Troparevsky2015a, Troparevsky2015b, King2016] have identified suitable compositional subspaces where single-phase HEAs might exist by additionally considering the enthalpies of competing intermetallic compounds. However, they too suffer from the drawback that "arbitrary" values of formation enthalpies of competing compounds have to be used to "predict" regions where single or multiple phases are stable.

In this connection it is worth noting that in many studies minimal effort is put into determining the reliability of the experimental observations used for the correlations described above. For example, many studies rely on X-ray diffraction (XRD) alone to determine the microstructural states of the alloys investigated, which has the potential of mistakenly identifying an alloy as a single-phase solid solution when small amounts of secondary phases may well be present. Nevertheless, given the vastness of the compositional space that HEAs occupy, such low-resolution techniques are probably unavoidable to perform a rough initial screening to identify which compositions might be worth investigating in further detail.

Notable high-entropy alloys. Single-phase solid solution HEAs with the face-centered cubic (FCC) [Cantor2004, Otto2013a, Gali2013, Otto2013b, Tsai2013, Liu2013, He2014, Gludovatz2014, Otto2014, Wu2014, Haglund2015, Laplanche2015a, Laurent-Brocq2015, Laplanche2015b, Ma2015b, Laplanche2016, Bracq2017, Laplanche2108a, Laplanche2018b, Haas2019], body-centered cubic (BCC) [Senkov2010, Senkov2011a, Senkov2011b,

Senkov2011c, Senkov2012, Senkov2014, Juan2015, Senkov2015, Couzinié 2015, Sheikh2016], hexagonal close-packed (HCP) [Takeuchi2014, Feuerbacher2015, Zhao2016, Soler2018, Qiao2018] and orthorhombic [Lilensten2014] crystal structures have been identified in the literature. Of these, the FCC and BCC alloys are the most extensively investigated ones by far and we limit the rest of our discussion to these two crystal structures. Within these, we focus our discussion on just a few model HEAs whose structure-property relationships have been carefully investigated to uncover salient features of their behavior.

The FCC CrMnFeCoNi (Cantor) alloy. The quinary CrMnFeCoNi alloy was one of the first equiatomic HEAs reported to crystallize as a single-phase FCC solid solution [Cantor2004]. Recently, however, it was discovered that it decomposes into metallic (BCC-Cr) and intermetallic ($L1_0$-NiMn and B2-FeCo) phases below about 800°C [Otto2016]. Some of these transformations occur very quickly when the alloy is in the nanocrystalline state [Schuh2015] but take longer in large-grained material [Pickeringa2016, Laplanche2018]. It is not known whether this difference is due to the grain boundaries providing favorable nucleation sites and/or faster diffusion paths. Regardless, after heat treatments above 800°C, the metastable FCC solid solution state can be retained at room temperature at "normal" cooling rates. Its microstructure has been examined at multiple length-scales using XRD [Otto2013a, Gali2013, Bhattacharjee2014, Salischev2014, Stapanov2015], scanning electron microscopy (SEM) [Gali2013, Otto2014, Laplanche2015b, Otto2016], transmission electron microscopy (TEM) [Otto2013b], electron backscatter diffraction (EBSD) [Otto2014Laplanche2015b], and atom probe tomography (APT) [Laurent-Brocq2015, Schuh2015]. Taken together, the results show that the alloy is a single-phase FCC solid solution with no indication to date of any clustering or short-range ordering, although if such local ordering is experimentally proven to exist, density functional theory (DFT) calculations suggest that it would have a profound effect on critical properties such as the stacking fault energy and dislocation mobility, and thus be a major factor in controlling mechanical properties [Ding2018]. After deformation processing and recrystallization, the crystallographic texture is weak and close to random [Laplanche2016]. At very low temperatures, below about 50 K, computations based on DFT show that the FCC structure of the Cantor alloy becomes unstable and transforms to the HCP structure [Ma2015a]. While there has been no direct confirmation of this temperature-induced phase transformation, two recent experimental studies indicate a pressure-induced transformation from FCC to HCP [Tracy2017, Zhang2017b].

Although the Cantor alloy dates back to 2004, it was not until almost a decade later that its malleability began to be appreciated and exploited. This enabled thermomechanical processing to be performed and, consequently, tensile tests to be performed for the first time on any high-entropy alloy [Gali2013]. Several important features of the Cantor alloy were revealed in that seminal paper [Gali2013]: (*i*) it exhibits a strong temperature dependence of strength below about 473 K, a weaker temperature dependence at elevated temperatures up to 1273 K, and a modest strain rate dependence at low homologous temperatures; (*ii*) its strength and ductility both increase with decreasing temperature down into the cryogenic range with ultimate strengths and elongations in excess of 1 GPa and 60%, respectively, at 77 K; (*iii*) its work hardening rate increases strongly with decreasing temperature, which postpones the onset and necking and thereby increases the tensile ductility; (*iv*) it fractures transgranularly by ductile microvoid coalescence, consistent with the high ductilities observed. As discussed later in this section, tests on single crystals of the Cantor alloy have confirmed the temperature dependence of yielding observed in polycrystalline samples.

Subsequent investigations characterized the dislocation structures and microstructural evolution with strain to obtain a fundamental understanding of the mechanical properties of the Cantor alloy. Multiple deformation mechanisms appear during tensile tests. The main findings are that slip initially occurs by planar glide of ½<110> dislocations on {111} planes [Otto2013b, Laplanche2016, Okamoto2016a]. The perfect dislocations split into 1/6<112> Shockley partials bounding a stacking fault with average splitting distances ranging from ~3.5-4.5 nm for the edge orientation to ~5-8 nm for the screw yielding a stacking fault energy (SFE) of 30 ± 5 mJ/m^2
[Okamoto2016a]. This experimental SFE is slightly greater than the 0 K value (18-27 mJ/m^2) computed using DFT techniques [Zaddach2013]. The relatively large partial separations (especially when normalized by the Burgers vector) imply that cross-slip is difficult in this alloy, which is consistent with the planar slip and long dislocation pile-ups observed at grain boundaries [Otto2013b]. At high magnifications, significant (factor of 2) local variations in the stacking fault widths are observed [Smith2016], likely due to local changes in the SFE related to local variations in composition. At lower magnifications, the dislocations are long and smoothly curved on the {111} planes without any preferred line direction implying similar mobilities of edge and screw segments [Okamoto2016a]. *In situ* straining in the TEM [Zhang_NatComm_2015] suggests that the Shockley partials appear to be more mobile than the perfect (undissociated) segments, which are very sluggish; the fast-moving partials are arrested

at the planar slip bands consisting of perfect dislocations. However, since no information is typically available in the TEM straining experiments regarding the local resolved shear stress acting on the moving dislocations, caution has to be exercised in making conclusions about the relative mobilities of the different dislocations seen during *in situ* observations.

With increasing strain at room temperature, partials are activated on multiple slip systems and those moving on inclined slip planes interact at their junctions; some of these interactions produce three-dimensional parallelepiped volume defects that act as further barriers to planar slip [Zhang_NatComm_2015] analogous to the stacking fault tetrahedra seen in FCC metals. The dislocation density increases from very low values in the recrystallized (unstrained) state to values of 2-4 $\times$ 10^{14} m^{-2} at strains of 15-20% [Laplanche2016]. Eventually, well-developed cell structures form at strains of 20% or higher [Otto2013b, Laplanche2016]. The work hardening rate decreases rapidly from ~G/20 (where G is the shear modulus) at the start of tensile straining to ~G/30 at approximately 8% true strain; beyond that, the work hardening rate continues to decrease, but less rapidly, to ~G/10 at 30% strain [Laplanche2016]. Thus, as in other FCC metals and alloys, dislocation mechanisms by themselves are insufficient to sustain a steady (non-decreasing) work hardening rate. At high applied stresses close to the fracture stress, twinning is finally activated [Laplanche2016] but it appears too late in the deformation process to prevent the onset of necking instability.

The microstructure evolution is distinctly different when the straining is carried out at cryogenic temperatures. At 77 K, the initial distribution of dislocations as well as their density evolution with strain is similar to that at room temperature [Laplanche2016]. Correspondingly, the work hardening rate decreases rapidly from ~G/20 at the start of tensile straining to ~G/30 at approximately 8% strain, similar to the behavior at room temperature. However, beyond that, twinning is activated, which provides an additional hardening mechanism. Correspondingly, the work hardening remains constant at ~G/30 from true strains of 8% to almost 40% [Laplanche2016]. The twins are nanoscale in their widths (~10-25 nm on average) and micrometer-scale in their spacing (mean values ranging from ~20 μm at 8% strain to ~1 μm at 45% strain) [Laplanche2016]. Assuming that the twin boundaries act like grain boundaries as barriers to dislocation motion, the decrease in twin spacing with strain is indicative of a "dynamic Hall-Petch effect" that provides hardening to counteract the softening due to dislocation recovery processes. This additional hardening mechanism is what is able to maintain a constant, steady work hardening rate at strains where dislocation hardening peters out.

Based on TEM investigations of samples taken from interrupted mechanical tests, twins were found to appear at true strains of ~7.5 at 77 K, but at much higher strains (~25%, close to fracture) at room temperature [Laplanche2016]. The corresponding tensile stresses were ~720 MPa at both temperatures, indicative of a temperature-independent twinning stress similar to what has been seen in many other materials [Meyers2001]. Dividing the polycrystalline twinning stress by the Taylor factor gives a critical resolved shear stress (CRSS) for twinning of about 235 MPa. This value has to be treated with caution because the polycrystalline material investigated had a relatively small grain size of 17 μm [Laplanche2016], and it is known that twinning becomes more difficult as the grain size is decreased [Meyers2001]. A better estimate could be obtained by testing material with larger grains. Furthermore, there are experimental uncertainties related to where in the gage section the TEM specimens are taken from and the limited volume examined by TEM (twinning may well have occurred at lower strains, but the sampling may have been insufficient to catch it).

Single crystals offer a more direct way to characterize twinning in the Cantor alloy [Abuzaid2017, Kireeva2017, Wu2018, Kireeva2018, Bönisch2018]. From a [111] oriented tensile specimen, the CRSS for {111}<112> twinning was determined to be~150 MPa at 77 K and it occurred on the twin system with the highest Schmid factor [Abuzaid2017]. Another [111] specimen tested at room temperature did not exhibit twinning, although it work-hardened extensively and experienced a stress higher than the twinning stress at 77 K. This latter observation suggests the possibility that the twinning stress may indeed depend on temperature, although to what extent remains unknown. Two other orientations were tested at 77 K, but they did not show twinning because the applied stress did not reach the twinning stress.

Consistent with its high strength and ductility, the Cantor alloy exhibits exceptional fracture toughness, as shown in Fig. 2 [Gludovatz2014]: its crack-initiation toughness (K_{JIc}) is ~220 MPa $m^{1/2}$, roughly independent of temperature from room temperature down to 77 K, while its crack-growth toughness exceeds 300 MPa $m^{1/2}$ at these temperatures (rising *R*-curve behavior). While increase in strength and ductility with decreasing temperature is seen in other FCC alloys (*e.g.*, austenitic stainless steels), the retention of high toughness at cryogenic temperatures makes the Cantor alloy unique since most materials become more brittle as the temperature is decreased. Twinning was observed in the highly stressed regions in front of the crack tip in the fracture toughness specimens tested at 77 K. In a follow-on *in situ* straining study

of this material in a TEM, twinning was observed in the crack-bridging ligaments behind the crack tip at room temperature [Zhang2015]. Twinning has also been observed in the Cantor alloy after high pressure torsion [Schuh2015] and rolling [Stepanov2015] both of which subject the material to high strains and stresses.

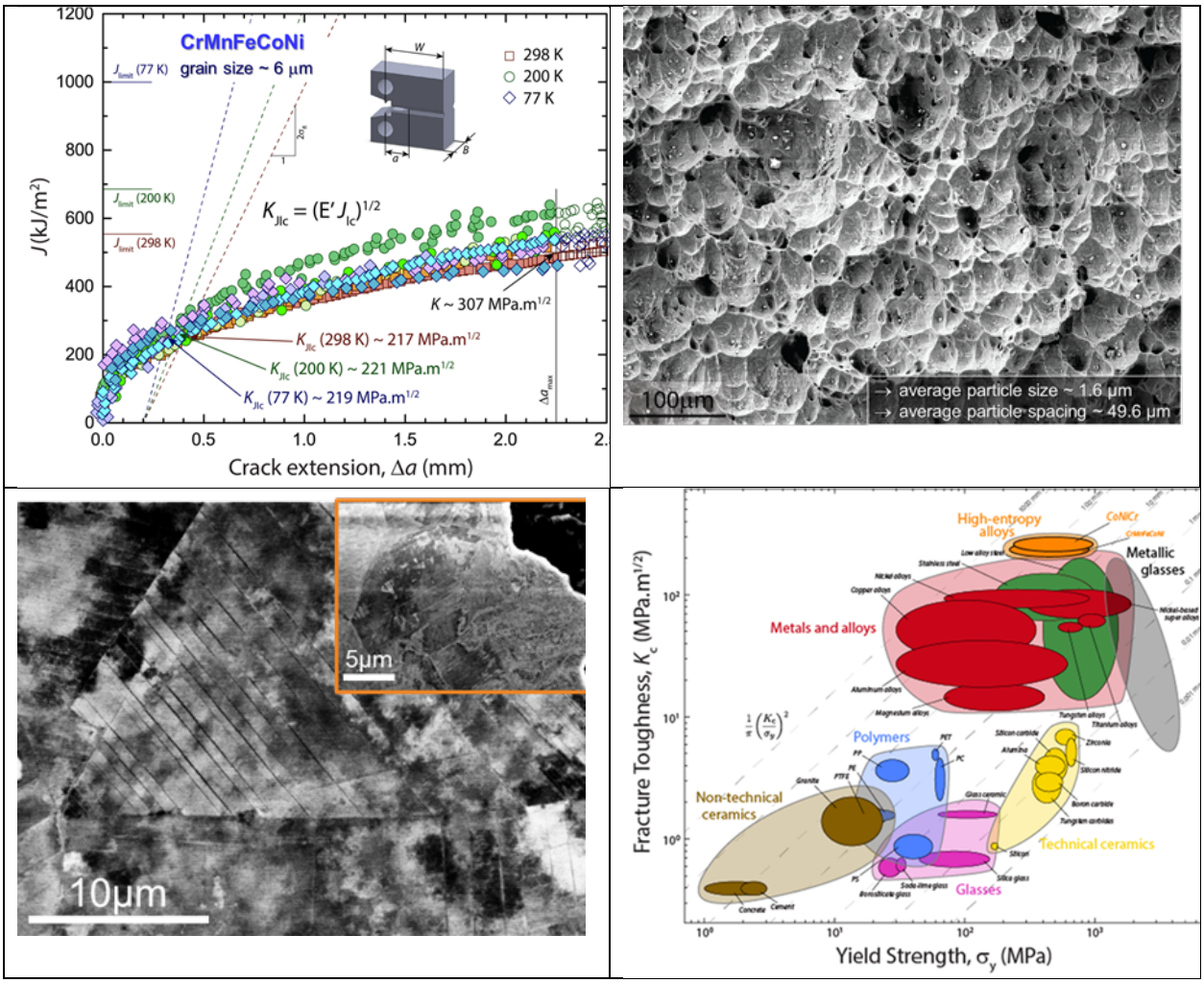

Fig. 2. **Damage-tolerant properties of the Cantor CrMnFeCoNi alloy.** (A) Fracture toughness crack-resistance curves show the alloy to display crack-initiation K_{Ic} toughness in excess of 200 MPa√m at ambient down to liquid-nitrogen temperatures, and "valid" crack-growth toughnesses above 300 MPa√m [Gludovatz, *et al*., *Science*, 2014]. Such exceptional toughness properties, which are even higher in the three-component CrCoNi alloy, are associated

with (B) a fully ductile microvoid coalescence mode of fracture, and (C) extensive deformation nano-twinning at 77 K (the roughly 10% stronger CrCoNi alloy deforms by twinning at temperatures as high as 293 K). (D) Ashby plot of strength *vs.* fracture toughness which show that these CrCoNi-based medium- and high-entropy alloys are among the most damage-tolerant materials on record [Gludovatz, *et al*., *Nature Comm*, 2016)].

From compression tests on a $[5\bar{9}1]$ oriented single crystal, the critical resolved shear stress (CRSS) for activation of {111}<110> slip in the Cantor alloy was first determined to be 70 and 175 MPa at room temperature and 77 K, respectively [Patriarca2016]. These values are higher than those estimated by dividing the polycrystalline yield stress by the Taylor factor: *e.g*., for a grain size of 155 μm, the yield stresses at room temperature and 77 K are ~170 and 350 MPa, respectively [Otoo2013b], from which upper limits of the corresponding CRSS can be deduced as ~55 and 114 MPa, respectively. Shortly thereafter, single crystal micropillar compression results were published [Okamoto2016a] which showed that extrapolation of the size-dependent strengths to pillar sizes of 20-30 μm gave values for the bulk CRSS of 33-43 MPa at room temperature that are more in line with the polycrystalline data. Additionally, the CRSS values were not orientation dependent (*i.e*., Schmid's law was valid for the $[\bar{1}26]$ and $[\bar{1}23]$ orientations tested). Subsequently, [111], [149], [122] and [123] oriented single crystals were tested in tension and CRSS values of ~55 and 150 MPa were obtained at room temperature and 77 K, again independent of orientation [Abuzaid2017]. As in the case of polycrystals [Gali2013, Otto2013b], the single crystal data show that strength increases significantly as the temperature is decreased from room temperature to 77 K. There are some differences between the CRSS obtained directly from single crystal tests and those obtained indirectly from polycrystal tests and micropillar compression tests, which may be related to the assumptions inherent in the indirect methods. However, the CRSS from the two single crystal studies are also different, which may be related to compositional variations or impurity effects.

A question that naturally arises is whether the temperature dependence of the CRSS (or of the yield or flow strength of polycrystals) is due to the temperature dependence of the shear modulus (G), given that strength is proportional to G in all strengthening models. However, G of the Cantor alloy shows relatively weak temperature dependence [Haglund2014], weaker than that of pure Ni, in the temperature range from room temperature down to 77 K where its yield strength increases dramatically while that of Ni is relatively flat. Therefore, the temperature dependence of G cannot be the reason for the temperature dependence of the CRSS.

Although the strong temperature dependence of the CRSS of the Cantor alloy between room temperature and 77 K stands in sharp contrast to the behavior of pure FCC metals such as

Ni, it is well known that solid-solution alloys, including binaries [Koppenaal1962, Basinski1972, Traub1977, Butt1978, Wille1986, Wille1987], exhibit temperature dependences that increase with increasing solute concentration. A new theory of solid-solution strengthening developed for concentrated alloys [Varvenne2016, Varvenne2017] quantitatively explains the temperature dependence of strength observed in the Cantor alloy and its FCC subsets [Wu2014].

The room-temperature CRSS at yield of the Cantor alloy is an order of magnitude greater than that of Ni (~3 MPa [Haasen1958]), which is an FCC metal with comparable melting point and shear modulus. This degree of solid solution strengthening cannot be reconciled in terms of the maximum difference (~1%) in the atomic (Goldschmidt) radii of the constituent elements. However, the effective atomic radii in the Cantor alloy can be calculated using DFT methods, and the maximum (pair-wise) size difference in that case turns out to be ~4% [Okamoto2016a]. Based on this, a hypothetical binary alloy with 4% mismatch, the shear modulus of the Cantor alloy, and a solute concentration in the range 20-50% was shown to have yield strengths comparable to the Cantor alloy [Okamoto2016a]. Because the constituent elements have different atomic sizes, their centers are displaced from the ideal FCC lattice points. The displacement of each element can be calculated using DFT methods [Okamoto2016b] and it depends on the local environment (that is, surrounding atoms). The computed mean square atomic displacement (MSAD) is largest for Cr (~43 pm^2) and smallest for Ni (~9 pm^2). Averaging the computed MSADs over the entire crystal gives a value of 25 pm^2 for the Cantor alloy. Experimentally, the atomic displacement of the individual elements is difficult to measure. However, using synchrotron X-ray diffraction, the atomic displacement parameter (ADP), which is the sum of the squares of the atomic displacements averaged over the entire crystal was determined to be ~24 and 59 pm^2 at 25 and 300 K, respectively [Okamoto2016b]. The ADP value at 25 K is representative of the static disorder in the Cantor alloy while the difference between it and the room temperature value is representative of the dynamic disorder due to thermal vibrations. The 25 K value is almost identical to the computed value (average of MSADs) and its square root gives the average displacement of the atoms in the Cantor alloy from their ideal lattice positions, namely 5 pm. This gives a sense of the lattice distortion (<2% of the Burgers vector) needed to get significant solid solution strengthening in the Cantor alloy. Of course, the displacements of the individual atoms can be more (~6.5 pm for Cr and ~5.5 pm for Mn), less (~4 pm for Co and ~3 pm for Ni), or about the same (~5 pm for Fe) as the displacement averaged over the whole alloy [Okamoto2016b].

Non-equimolar and multi-phase derivatives of the Cantor alloy. Based on the equimolar Cantor alloy, several related variants with fewer alloying elements or non-equimolar compositions have been developed. One of the rationales was to reduce the stacking fault energy to promote TWIP [Deng2015, Li2017a] and/or TRIP [Li2016, Li2017b] and, thus, to realize materials with superior strain hardening potential.

One effective approach has been to simply remove elements from the Cantor alloy, the most notable examples being the equiatomic medium-entropy alloy CrCoNi [Wu2014, Zhang2017b, Zhao2017] and the related ultrastrong alloy VCoNi [Sohn2019]. These single-phase FCC alloys appear to be similar to the five-element Cantor alloy, only with enhanced strength and ductility [Wu2014, Sohn2019] and toughness [Gludovatz2016]. Indeed, at 77 K, CrCoNi (with 5 to 50 μm grain size) displays tensile strengths approaching 1.4 GPa, tensile ductilities of ~90%, and fracture toughness values of ~270 MPa $m^{1/2}$ at crack initiation and exceeding 400 MPa $m^{1/2}$ for crack growth, making it one of the most damage-tolerant materials on record [Gludovatz2016]. Its lower stacking fault energy and higher yield strength (compared to the Cantor alloy) allows it to reach the twinning stress more easily, resulting in profuse nano-twinning even at room temperature (Laplanche2017). The twin boundaries act to arrest dislocations that impinge upon them, yet the boundaries themselves act as pathways for the glide of partial dislocations, respectively promoting strength and ductility [Zhang2017b]. Significant increases in the yield strength of the single-phase CrCoNi alloy to values exceeding 1 GPa have been achieved by cold work followed by partial recrystallization [Yang2018, Slone2019] albeit at the sacrifice of tensile ductility (to 20-30%). Precipitation of a second phase with the $L1_2$ crystal structure can also enhance the yield strength of CrCoNi (to ~800 MPa, somewhat lower than by cold work) while maintaining tensile ductility in excess of 40% [Zhao2017]. However, since the precipitate type, volume fraction, and size distribution were not optimized, there remains room to further enhance the strength-ductility combination of CrCoNi-based alloys.

Another approach [Deng2015, Tasan2014, Wang2018, Li2017c] involved developing a non-equiatomic $Fe_{40}Mn_{40}Co_{10}Cr_{10}$ high-entropy alloy that deformed by planar dislocation slip early on and by mechanical twinning at larger strains (>10%) at room temperature. In the equimolar Cantor alloy, such TWIP has only been observed under cryogenic conditions or after the application of very high strains, as discussed before. A group of novel non-equiatomic multi-component CoFeMnCrNi alloys that form planar slip substructures at strains <2% and complex cell structures with high dislocation-density walls at higher strains (up to 45%) was also developed [Pradeep2015]. Its strain hardening properties were similar to those of the Cantor alloy, but it used lower-cost alloying elements.

Experiments [Li2016] on a set of Cantor-related HEAs with composition $Fe_{80-x}Mn_xCo_{10}Cr_{10}$ where the Mn content was varied between x = 30 at.% and 45 at.% (Fig. 3) showed that, whereas the Mn-rich alloy (45 at.%) deforms by the development of complex dislocation patterns, the 40 at.% Mn variant is a TWIP alloy and the 35 at.% Mn variant is a TRIP alloy, reflecting the influence of the reduction in stack-faulting energy with decreasing Mn content. The 30 at.% Mn variant is an alloy consisting initially of two HEA phases, an FCC and an HCP phase. As both phases are massive solid solutions, the alloy was termed dual-phase HEA. The FCC phase is metastable, so it partially transforms into HCP martensite upon loading (Fig. 3). Alloys consisting of two such (metastable) HEA phases, notably FCC and HCP, are characterized by a near-zero stacking-fault energy. This feature was recently shown to enable not only a forward TRIP effect from the FCC to the HCP phases but also local reverse transformation back into the FCC phase. This mechanism, which seems to proceed through the forward and backward motion of individual partial dislocations, was referred to as the bidirectional TRIP (B-TRIP) effect, and it substantially refines the microstructure down to a nanolaminate-type substructure [Lu2018]. The associated high interface density reduces the dislocation's free path, hence enhancing the strength of the material (Box 2).

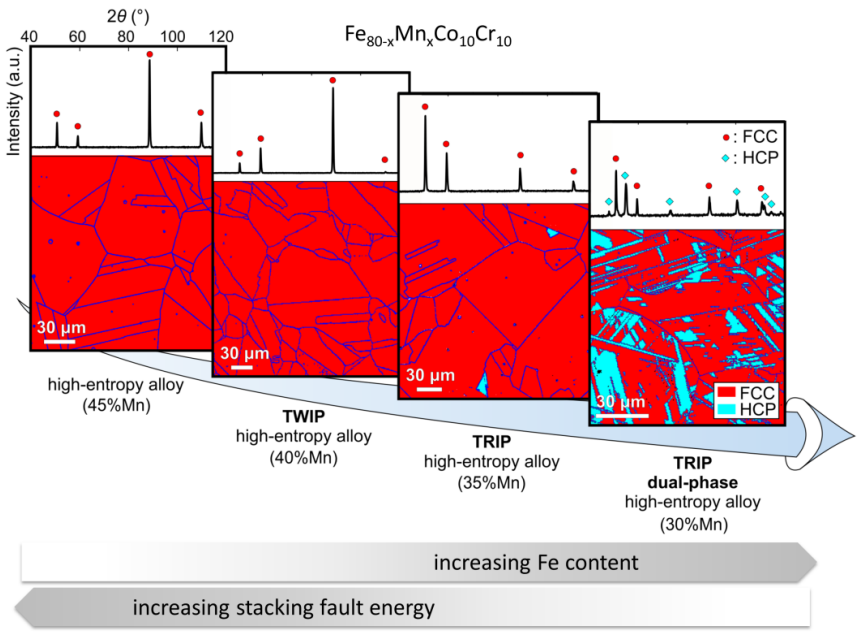

Fig. 3. Change in the phase fractions (FCC: red; HCP: blue) for the alloy system $Fe_{80-x}Mn_xCo_{10}Cr_{10}$ and the associated dominant deformation mechanisms. Image taken from [Li2016].

Alloy variants that underwent similar, sequential, activation of athermal, deformation-driven transformation to provide additional strain hardening have also been realized through interstitial alloying [Li2017c, Wang2018, Su2019], using knowledge from TWIP and TRIP steels.

These examples of Cantor alloy variants demonstrate that modest deviations from the equimolar compositions originally prescribed for HEAs can be utilized for compositional tuning of the stacking-fault energy. Through this approach, thermodynamically-guided strain-hardening engineering can be accomplished, enabling the activation of beneficial strain-hardening features including stacking faults, reactions among partial dislocations, complex dislocation patterns, twinning and martensite formation.

The BCC TiZrHfNbTa alloy. Compared to the extensive information available on the FCC Cantor alloy and its derivatives, little is known about the fundamental structure-property relationships in BCC HEAs, especially the refractory HEAs. This is mainly due to their brittleness and high melting points, which we refer to as Senkov alloys because of Oleg Senkov's leading role in identifying and developing them. The paucity of data on refractory HEAs in mainly due to their brittleness and high melting points, which make it difficult to break down their cast, dendritic microstructure and produce material with homogeneous structure and

composition. The exception is the equiatomic Senkov alloy TiZrHfNbTa, which is the only one that exhibits tensile ductility at room temperature [Senkov2015, Dirras2016]. It was first synthesized in 2011 by arc melting followed by hot isostatic pressing, after which it had a dendritic microstructure [Senkov2011c]. XRD studies indicated that it was mostly single-phase BCC with one minor extra peak that the authors thought belonged to a hexagonal phase [Senkov2011c]. The lattice parameter of the BCC phase was determined to be 0.3404 nm, close to the 0 K value computed by DFT methods of 0.339 nm [Song2016]. Subsequent research [Couzinié2014] looked at the alloy after arc and induction melting in a water-cooled Cu crucible and found only BCC peaks in the XRD spectrum which yielded a comparable lattice parameter of 0.3401 nm. The alloy had a dendritic microstructure near the surface that was in contact with the argon atmosphere (where the cooling rate was relatively slow), which disappeared near the surface in contact with the copper (where the cooling rate was high). The dendrite arms were enriched in Ta and Nb (which have the highest melting points) while the interdendritic regions were enriched in the lower melting point elements Ti, Zr and Hf. The solidification zone that was devoid of dendrites appeared to be free of segregation. TEM analysis confirmed that the alloy was single-phase BCC at the microscopic scale [Couzinié2014]. Similar dendritic segregation was observed in another study [Lin2015] which also reported a comparable lattice parameter (0.3414 nm).

The cast TiZrHfNbTa alloy was tested initially in compression from room temperature to 1473 K [Senkov2011c, Senkov2012] and then in tension at room temperature [Dirras2016]. Depending on the location within the casting from where the tensile specimens were cut, significant variations in the room-temperature tensile stress-strain curves were observed [Dirras2016], which was ascribed to the different degrees of dendritic segregation and other casting defects such as porosity in the different regions. Yield strengths ranged from 790 to 805 MPa, followed by modest strain hardening [Dirras2016]. It appeared that regions exhibiting greater degree of dendritic segregation were slightly stronger [Dirras2016], but the paucity of data makes it difficult to make robust conclusions at this time. Tensile ductilities ranged from ~6 to 9% and showed no clear correlation with strength [Dirras2016], suggesting that the influence of casting defects may be dominant. Prior to fracture, the specimen exhibited necking and post-rupture examination showed that the fracture surface was transgranular and covered in dimples of various sizes [Dirras2016]. TEM analysis after interrupted compression tests [Dirras2015] revealed that at small strains, deformation was localized in small bands bounding dislocation-

free regions. With increasing strain, the number of bands as well as the dislocation density in the bands increased. X-ray line profile analyses yielded values for the dislocation density of 1.5×10^{15} m^{-2} at compressive strains of 20%. The Burgers vectors were of the ½<111> type and the dislocations became more screw in nature with increasing strain [Dirras2015], indicating that their mobilities were lower than those of edge dislocations, similar to observations in other BCC metals. Consistent with the Peierls mechanism and strong intrinsic lattice resistance, the activation energy for plastic deformation obtained from room-temperature stress relaxation experiments was around $50b^3$ at yield, which decreased slightly to around $30b^3$ at 20% plastic strain [Couzinié2015], where b is the magnitude of the Burgers vector. For comparison, the FCC Cantor alloy has a much larger activation volume at yield of ~$350b^3$, which decreases to ~$150b^3$ at ~20% plastic strain [Laplanche2018].

A major advance in the study of BCC HEAs was the discovery that the TiZrHfNbTa Senkov alloy can be heavily cold rolled (~86% thickness reduction) and recrystallized [Senkov2015], which opened the door to thermomechanical processing and grain size control [Juan2015]. Tensile tests on material with ~30 μm grain size gave yield and ultimate stresses of 1145 and 1262 MPa, respectively, and elongation to fracture of 9.7% [Senkov2015]. The fracture mode was mainly intergranular, but regions of ductile transgranular fracture were also observed [Senkov2015]. A subsequent study [Juan2015] investigated larger grain sizes of 38, 81 and 128 μm and obtained yield strengths of 958, 944 and 940 MPa. The Hall-Petch line drawn in that study if extrapolated to smaller grain sizes falls significantly below Senkov and Semiatin's yield strength of 1145 MPa [Senkov2015]. Additional work is needed to understand the reason for the discrepancy between these two recent studies. Juan *et al*. reported elongations to fracture of 15, 18, and 20% for grain sizes of 128, 81, and 38 μm, which is consistent with the textbook notion that grain refinement can simultaneously increase strength and ductility (for grain sizes that are not in the nanoscale regime). However, it is at odds with the lower tensile ductility (9.7%) reported in [Senkov2015] for 22 μm grain size, which should have had a higher ductility. This is another discrepancy that needs further work to be resolved.

As in FCC HEAs, TRIP effects can be advantageously used in BCC HEAs. The first work [Lilensten2017] to show this effect investigated an off-equiatomic metastable variant of the TiZrHfNbTa alloy, $Ti_{35}Zr_{27.5}Hf_{27.5}Nb_5Ta_5$, that was designed using the so-called bond-order,

d-orbital approach originally developed for Ti alloys. In BCC HEAs, this approach was used to promote a stress-induced transformation from the parent BCC phase to an orthorhombic α" martensite during deformation. The new alloy (referred to as Ti_{35} to distinguish it from the equiatomic alloy Ti_{20}), was produced by melting, casting, cold rolling, and recrystallization, and had a single-phase BCC structure with a grain size of ~40 μm [Lilensten2017]. Its yield strength, 540 MPa, was significantly lower than that of the equiatomic alloy produced similarly by cold rolling and recrystallization, 958-1145 MPa for grain sizes of 38-22 μm [Juan2015, Senkov2015]. However, its elongation to fracture was much higher (~23% in Lilensten2017 versus ~10% in Senkov2015]. Compared to the equiatomic alloy [Couzinié2015], which shows a monotonic decrease in the work hardening rate with strain, the work hardening rate of the Ti_{35} alloy, after an initial decrease, starts to increase sharply at a plastic strain of ~2%. This inflection point corresponds to the start of the BCC-martensite transformation responsible for the TRIP effect. With increasing strain, the amount of martensite increases (saturating at ~65%) and the martensite shows evidence of internal twinning [Lilensten2017]. Together, these TRIP and TWIP phenomena enable the Ti_{35} alloy to undergo extensive work hardening and reach an ultimate tensile strength comparable to that of the equiatomic alloy but with twice the tensile ductility. Subsequently, a similar TRIP effect in off-equiatomic quaternaries of the Ti-Zr-Hf-Ta system was demonstrated [Huang2017].

Although alloy design concepts based on metastability enable substantial gains in strain hardening and ductility through TRIP and TWIP effects, they are effective only at room- or modestly elevated temperatures. Thus, for improved creep properties, the use of dispersions of larger amounts of stable second phase particles seem to be a more promising design avenue for this alloy family. Also, at elevated temperatures and in harsh environments, the BCC refractory-element alloys would require adequate coatings and improved oxidation resistance to survive for long periods of time.

As in some of the FCC HEA systems, in which a beneficial effect of interstitial blending with C was observed, an anomalous interstitial strengthening effect of O was found in the single-phase equiatomic BCC TiZrHfNb alloy family [Lei2018]. Interstitial O remarkably improved the mechanical properties of this alloy at room temperature: the tensile strength increased by 48% and the tensile ductility increased by 95% with 2 at.% oxygen doping of TiZrHfNb. The O forms

ordered complexes that simultaneously pin dislocations and promote their cross slip and multiplication.

Finally, similar to the FCC Cantor alloy, the solid solution state of the BCC TiZrHfNbTa alloy is metastable at intermediate temperatures. Cold rolling followed by annealing at 800 °C resulted in two BCC phases and significant embrittlement relative to the single BCC phase obtained by cold rolling and annealing at 1000 °C [Senkov2015]. Another decomposition was observed when the rolled sheet was annealed for 2 h at 1200 °C; however, the low volume fraction of the precipitates, which formed both within the grains and on grain boundaries, meant that its nature could not be identified [Senkov2015]. After severe plastic deformation by high-pressure torsion at room temperature and annealing between 500 and 800 °C, decomposition into a Nb-Ta rich BCC phase and Zr-Hf rich HC phase occurred at lower temperatures followed by the formation of a Zr-Hf rich BCC phase at higher temperatures [Schuh2018]. This decomposition resulted in severe embrittlement, similar to that seen before [Senkov2015]. After annealing at 1000-1100 °C, only a single BCC phase remained, consistent with the earlier observation in cold rolled and annealed material [Senkov2015]. Similar phase transformations were observed also in cast material [Stepanov2018] indicating that they are thermodynamically stable phases that appear in various processing routes. For high-temperature applications, such transformations and their associated deleterious effects on mechanical properties are a concern and need to be carefully accounted for in the future. For relatively low-temperature applications, metastable microstructures are fine because of slow kinetics (steels and their myriad metastable variants are good examples). Sometimes metastability may even be desirable as in the case of the TRIP/TWIP alloys. However, for relatively long-term applications at elevated temperatures, one cannot rely on kinetic stabilization; the alloys have to be thermodynamically stable under service conditions.

Uncharted HEA space

If we consider that there are about 60 usable elements in the Periodic Table, the number of possible new, equiatomic five-element HEAs exceeds 5 million; if we contemplate alloys with different numbers of elements, or with non-equiatomic compositions, the number of potential new alloys becomes practically unbounded. The question that immediately arises then is how best to interrogate such a vast, uncharted HEA space. There is no simple answer to this question, as any envisioned solution will, by definition, have severe limitations: the expression

"finding a needle in a haystack" is particularly apt here.

Nevertheless, we consider here three different, nominally high-throughput, screening approaches: one based on purely computational studies, that is, using CALPHAD-type analyses [Gorsse2018, Zhang2012], another using an experimental combinatorial approach [Li2018b], and a third, more traditional approach based on mechanistic understanding to adjust the compositions and properties of known alloys [Li2017a].

Broad CALPHAD-type approaches

CALPHAD stands for CALculation of PHAse Diagrams, an acronym for thermodynamic models that derive equilibrium phase diagrams based on analytical Gibbs-Helmholtz free energy formulations for every phase. The models are cast in polynomial form, referred to as Redlich-Kistler functions, which allows us to readily take first and second derivatives that are needed to identify, for instance, spinodal phases. The parameters of the polynomials must be fitted using any available and reliable experimental and theoretical data, such as *ab initio* derived enthalpies, calorimetry data, metallographic results, or statistical models for the entropy. When the free energy approximations for each of the phases in an alloy system as a function of the relevant state variables, typically concentration and temperature at constant pressure, are identified, the thermodynamic equilibrium phase for each temperature is calculated by energy minimization using software from, for example, ThermoCalc or CompuTherm. This information is used to trace the phase diagram. It allows the identification of coexisting phases as well as their compositions and volume fractions. This methodology is currently being expanded to alloy systems with a high number of components, targeting particularly the CrMnFeCoNi Cantor system [Gorsse2018]. The Redlich- Kistler functions in these cases also include higher-order interaction parameters according to the number of components considered. Outside of the fitted ranges and for cases in which unknown competing intermetallic phases appear, this approach currently has limited predictive power.

Therefore, CALPHAD methods can only serve as a first, albeit important extrapolation step into unchartered compositional territory, as very often intermetallic phases appear. An additional approach might be to also screen compositional regions of interest for competing intermetallic phases that have high energy of formation, a task that is tractable with ab initio methods

[Troparevsky2015a, Troparevsky2015b].

A problem of the CALPHAD method is that being based on thermodynamics, it may miss all the metastable microstructural constituents and transient phase states that are at the core of the most successful engineering alloys. Examples are the martensite, bainite, pearlite or Guinier-Preston zones. Quoting from an earlier review [Pickering2016b]: "One can envisage that rapid approaches might miss most steels (had they not yet been discovered), due to their polymorphism and tendency to form brittle martensite when cooled quickly."

Moreover, as with the concept of the Materials Genome Initiative [Holdren2011], an initiative to accelerate the discovery and deployment of advanced materials, equilibrium approaches alone tell us little about the microstructure, morphology, size, distribution and orientation of the phases present, which control the structure and mechanical properties of the most successful alloys. Indeed, it has consistently been the plague of metallurgists in the development of new structural materials that most theoretical methodologies are not capable of reliably predicting the type and role of microstructures, which are such dominant factors in the control of mechanical properties.

Combinatorial experimental approaches

Since at least the mid-1960s, combinatorial approaches, which involve high-throughput synthesis and characterization of multiple-alloy compositions, have been used in materials science to rapidly determine phase diagrams in multi-component space, and screen physical and mechanical properties [Kennedy1965, Hanak1970, Xiang1995, Specht2003, Collins2003, Rar2005]. At least portions of the available compositional space can be surveyed by the fabrication and subsequent characterization of many alloy variants simultaneously [Pradeep2015, Wilson2016, Borkar2016, Li2018b].

Among the different combinatorial methods, four approaches have proven to be particularly useful for HEAs: bulk rapid alloy prototyping [Springer2012], diffusion couples and diffusion multiples [Zhao2005, Zhao2006], laser and electron additive manufacturing of compositionally graded samples [Knoll2017], and combinatorial thin-film materials libraries [Mertens2004, Ludwig2008].

Rapid alloy prototyping is a combinatorial bulk processing approach in which secondary specimens can be cut from processed sheets, e.g., for uniaxial tensile testing. The method

essentially comprises fast bulk processing steps, such as slab or strip casting, hot rolling, homogenization, cold rolling and recrystallization. Each casting can in itself be compositionally homogeneous or contain chemical gradients along the casting direction, introduced for instance by gradually blending a base alloy during an ongoing continuous casting process. This approach has the advantage of providing bulk samples with representative microstructures but is slow compared with thin film combinatorial methods, which can routinely synthesize multiple thin-film materials libraries by depositing thin-film composition gradients across a substrate in a single multi-target sputter experiment. Diffusion multiples, in which specimens with different compositions are brought together at elevated temperatures to produce chemical gradients across their interfaces [Zhao2005], and compositionally graded additive manufacturing methods [Dobbelstein2019] are located between rapid alloy prototyping and thin film methods, and provide access to mesoscopic and millimeter-sized specimens for subsequent property assessment.

Metallographic or XRD characterization of these miniature samples should then be used to yield important information about the phases and microstructures present. For small-scale combinatorial samples, nano- and micro-indentation testing can be used for probing the hardness of the alloys. Disadvantages of small-scale combinatorial methods include limitated product size, sometimes too small for a comprehensive screening of functional and/or mechanical properties (such as strain hardening, ductility or fracture toughness), and resulting materials that are too artificial in terms of microstructure, morphology, size, distribution and orientation of the phases present. Nevertheless, such combinatorial approaches can be valuable in eliminating impractical materials, such as hopelessly brittle alloys, and thus can play a key role in reducing the number of alloys to be considered in larger-scale evaluations, such as uniaxial tensile or fracture toughness tests, which are performed on more realistic product forms.

Mechanism-based HEA design approaches

Mechanical properties. An alternative to the systematic composition-screening of new HEAs is a microstructure-based and mechanism-based design approach. Traditional load-carrying materials such as steels and aluminum alloys use specific strengthening mechanisms, which depend on temperature, stress and strain rate. Engineering a material's response over a more complex load path requires using not one effect alone but a sequence of mechanisms, including their interplay and associated windows of operation.

Examples of materials treated this way are FeCrNi-based stainless or FeMnC-based TWIP steels, two alloy classes with some similarity to FCC HEAs [Raabe2015]. These materials are strengthened using mechanisms including marked solid-solution and precipitation strengthening, deformation twinning and the formation of ε-martensite and α-martensite phases. The presence of solid solutions in these alloys not only strengthens the matrix but allows also for tuning of the stacking fault energy, whose magnitude affects the formation of partial dislocations and the occurrence of planar slip and double cross slip. This promotes the formation of rigid dislocation reaction products, enhanced dislocation storage rates, slip patterns and evolving complex dislocation substructures [Raabe2016]. Reducing the stacking-fault energy promotes the onset of twinning or martensite formation in the desired deformation, stress and strain rate window [Christian1995, Steinmetz2013]. Nucleation of athermal transformation carriers depends also on the dislocation substructure [Venables1964, Friedel1965, Mahajan1971, Mahajan1973]. The key thermodynamic quantity for tuning all these features is the stacking-fault energy, which can thus serve as a reliable parameter for alloy-design.

In a mechanistic design approach, the sequence of mechanism activation is also important. For optimal strain hardening, dislocations alone are often not sufficient because their multiplication rate eventually saturates and work hardening varies only as the square root of dislocation density. Reducing the stacking-fault energy enables the activation of mechanical twinning when the strain hardening due to dislocations becomes weak. When the additional strain hardening provided by mechanical twinning also gets exhausted, martensite formation can be activated if the stacking-fault energy is sufficiently low (< 20 mJ/m^2) [Ma2015b, Gutierrez-Urrutia2012, Su2019]. Thus, sequential activation of strain hardening mechanisms can be the pathway for obtaining materials with high formability, all tuned by the same quantity, in this case, the stacking-fault energy [Zaddach2013, Huang2015].

Related design ideas based on different key tuning parameters can be gleaned from the treatment of maraging steels: in that case, it is essential to precipitate intermetallic phases with good matrix coherency, enabling extremely high nucleation rates resulting in nm-scale precipitation combined with sufficient antiphase boundary energies for high dislocation-cutting stress. In aluminum alloys, a mechanical response is designed via the transition from early stage spinodal decomposition to the formation of semi-coherent or incoherent second-phase particles for exploiting strain hardening by particle cutting or Orowan looping.

These examples show that mechanistic alloy design consists not only of targeting certain sets of deformation mechanisms and their sequential activation but rather in identifying and tuning the underlying thermodynamic and structural parameters that govern them. These parameters can be properties such as the stacking-fault energy, lattice coherency or Landau-type spinodal energy landscapes.

One approach to HEA design thus lies in translating and applying these mechanistic design rules to HEAs with the aim of preserving on the one hand their characteristic advantages such as massive solid solution and on the other hand combining them with the key mechanisms described above (Fig. 4).

A mechanistic approach to the design of HEAs is practicable owing to their high solid-solution content. This means that the design of, for instance, certain spinodal forms, stacking-fault energies or coherent precipitate phases can be achieved by an appropriate choice and quantity of the solid-solution elements that are present anyway in HEAs (Fig. 4) [Li2016, Li2017a].

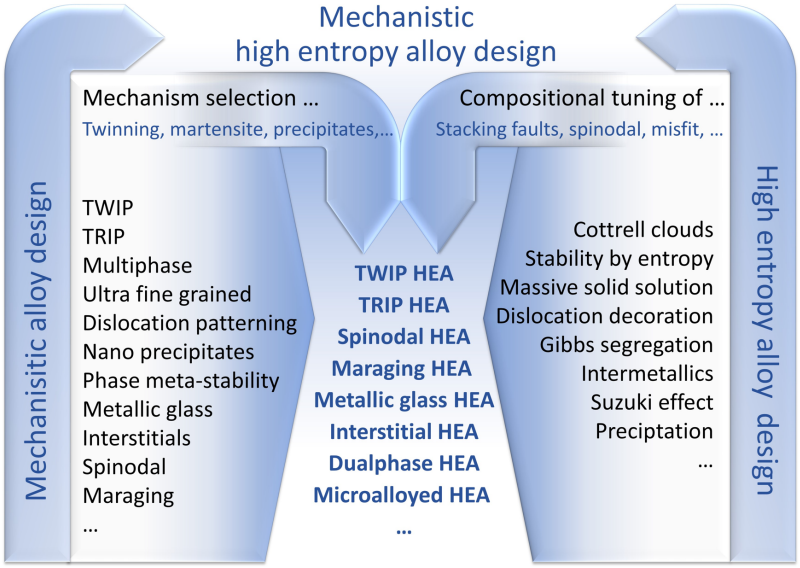

Fig. 4. A mechanistic approach to the design of HEAs. Established effects from conventional alloys such as the TWIP or the TRIP effects (left hand side) are combined with massive solid solution and its associated degrees of freedom for compositional tuning of stacking fault energy or desired precipitates (right hand side) for the design of several types of new HEA classes.

By taking such a mechanistic perspective, we are thus suggesting a targeted development of HEA variants such as TWIP, TRIP, maraging, martensitic or dual-phase HEAs, as well as

high-entropy superalloys or spinodally decomposing HEAs. Some of these material design ideas have already been realized and TWIP [Deng2015, Li2017a], interstitial [Li2017c, Wang2018, Li2018], TRIP [Li2017d, Basu2018] and dual-phase HEAs [Li2017b, Li2017d, Nene2017] have been obtained, in part also combining different defects depending on the magnitude of the stacking-fault energy (Fig. 5) [Li2016, Lu2018].

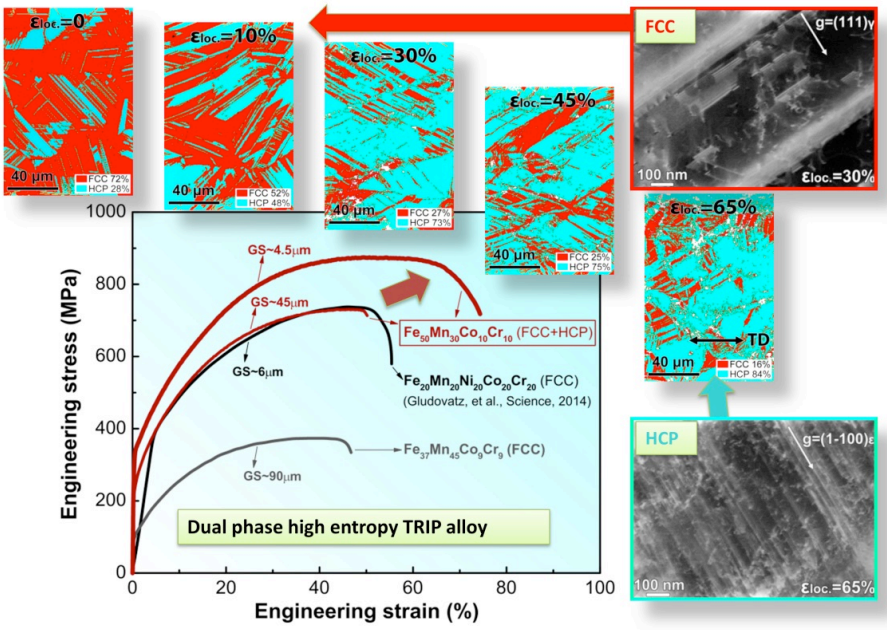

Fig. 5. Engineering stress-strain curve, associated phase maps (red: FCC; cyan: HCP) and two exemplary dislocation substructures mapped by using Electron Channeling Contrast Imaging (ECCI) for the HEA Fe50Mn30Co10Cr10 (upper curve) for two different grain sizes (GS). The phase maps reveal the presence of the two phases prior to loading and the gradual martensitic transition from FCC to HCP at room temperature during tensile deformation. In the ECCIs, **g** is the diffraction vector. Inage taken from [Li2016].

It should be noted that in several of these mechanistically designed alloys, some of the original HEA rules were violated: for example, fewer than five alloying elements were used, along with minor alloy ingredients at levels below 5%. Allowing for such compositional deviations from the original HEA rules is justified: first, the mixing entropy curves have a shallow shape so that deviations from equimolar compositions do not alter the configurational entropy substantially; second, compositional tuning of the stacking fault energy, or other key thermodynamic parameters, is far more important than maximizing

entropy; third, when striving for mechanical properties, avoiding brittle intermetallic phases is more of an imperative than obeying static alloy design rules. The latter point is particularly pertinent as many HEAs with an equimolar composition contain one or more intermetallic phases, which can render them brittle.

Functional properties. Although some HEAs have superior mechanical properties, such as high fracture toughness under cryogenic conditions [Gludovatz2014] and excellent strength and ductility combinations [Laplanche2016, Li2016, Li2017b] that are consistent with the mechanisms laid out above, only in a few cases will HEAs find their place in the materials selection portfolio based on their mechanical properties, simply because it is hard to surpass established materials such as steels, titanium alloys or nickel-based superalloys in terms of stiffness, strength, ductility, toughness or creep resistance. Thus, the long-term goal of HEA research cannot lie in merely reproducing properties that can already be achieved by well-established, less expensive competitors.

Accordingly, we believe that the development of future HEAs should also focus on achieving a multi-functional behavior to marry specific functional properties to the excellent mechanical properties of many of these alloys. As such, the importance of HEAs may well lie in the ability to design unprecedented combinations of mechanical and functional properties in the versatile and seemingly unlimited space of new alloy compositions. In the past, sufficiently ductile and mechanically strong alloys with additional functional features have often enabled application breakthroughs. Traditional examples include steels containing more than 12 wt.% Cr that are strong and corrosion resistant, FeNi Invar alloys with negligible thermal expansion in certain temperature ranges, soft magnetic FeSi-based alloys with small hysteresis losses, NiTi-based superelastic and shape-memory alloys with good thermomechanical properties, and Nb_3Sn type II superconductors with both a high transition temperature and high critical field.

Thus, promising targets for the future development of HEAs include functional properties related to corrosion, hydrogen embrittlement resistance [Luo2017, Luo2018], stress corrosion resistance, weldability [Nene2017], weight reduction, enhanced elastic stiffness or tailored elastic anisotropy, soft and hard magnetic features, combined magnetic and invar response, specific electrical resistivity, magneto-resistivity and electro-migration resistance, shape memory features, thermoelectric energy harvesting capabilities, superconductivity [Kozelj2014, Vrtnik2017], surface oxide layers with desired semiconductor features, self-healing or self-reporting bulk or surface behavior, anti-fouling or anti-bacterial surfaces oxide layers, biocompatibility, bioresorption, and properties relevant for anodic battery materials. These properties are to a certain extent available from different materials, but often not in a well-tailored fashion and not combined with excellent mechanical properties at extreme temperatures and environmental conditions, low price and good processing behavior.

HEAs may open additional pathways for blue-sky research, specifically for less mechanistically-driven studies that are open to unexpected property discoveries. The design and use of quantum mechanically guided HEA treasure maps that point towards promising compositions for functionally oriented structure-property relationships will be helpful in this regard.

In the past few years, papers on materials that might be broadly classified as "high-entropy ceramics" with the potential for interesting functional properties have begun to appear. Examples include oxides, carbides, nitrides and diborides.

Prospects and future opportunities

HEAs have taken the field of materials science, or more precisely metallurgy, by storm; indeed, they are likely to be central to the field of structural, and perhaps functional, materials for another decade or longer. As we discussed, the high-entropy phenomenon has been principally driven by three main factors: the exceptional mechanical properties of a few specific alloys, most notably the FCC CoCrNi-based alloys, especially for cryogenic temperature applications; the search for new refractory HEAs that can operate with sustained strength at ever increasing temperatures, a difficult pursuit because of the limited ductility and oxidation resistance of these materials; and the prospect of discovering new materials with unprecedented properties, or combinations of properties, from the seemingly unbounded list of possible multiple principal element materials, although this is a non-trivial exercise in light of the

methods currently at our disposal to venture into uncharted material, composition and microstructural space. At present, it is clear that the literature has been dominated by the first factor as the Cantor alloy and its derivatives have displayed truly compelling mechanical properties, coupled with now several successful attempts at microstructural optimization of these alloys and new mechanistic interpretations to underpin their impressive mechanical performance. However, we suspect that the latter two factors will ultimately come *to the fore* as the quest for higher temperature structural materials remains a perennial activity in materials science, invariably driven by advances in aerospace and now hypersonic activities, and the possibility of the discovery of new, hitherto unknown, 'super materials' will forever be a worthy cause.

However, in the short term, several specific issues remain to be resolved pertaining to what may make HEAs distinct from conventional alloys. One is the role of local chemical order on the macroscopic properties of HEAs. DFT-based Monte Carlo simulations on equimolar CoCrMo with several hundred atoms [Ding2018)] and molecular dynamics simulations with a few million atoms using a newly developed classical potential for CoCrMo [Q-J. Li, E.Ma, H.Sheng, unpublished (2018)] both predict that the degree of local chemical order in CoCrNi has a marked influence on its stacking-fault energy (Fig. 6), twinning energy, energy difference between the FCC and HCP phases (which governs the TRIP and TWIP effects), and formation energy for point defects, all of which are parameters that are known to markedly affect the strength and deformation of CoCrNi-based HEAs. However, the role of local chemical order in HEAs remains an open issue because it has yet to be convincingly confirmed experimentally. Only one study [Zhang2017a], using Extended X-ray Adsorption Fine Structure on CrCoNi has suggested that Cr atoms display a preference to bonding to Ni and Co atoms, rather than other Cr atoms, which is consistent with the DFT-based Monte Carlo predictions. However, the fascinating notion of tuning atomic order to achieve enhanced macroscale mechanical properties awaits more convincing experimental confirmation that such local chemical order actually exists in apparently random HEA solid solutions.

Further opportunities lie in the exploration of thermodynamics, microstructure evolution and properties of HEAs with near-zero stacking-fault energies. Metastable HEAs with small stacking-fault energy and deformation-driven twinning and martensite formation have been

studied; yet, even more complex substructures have been recently reported for dual-phase FCC/HCP HEAs with near-zero or slightly negative stacking-fault energy. In these materials, the matrix can assume both the HCP and the FCC structure, owing to the energetic equivalence of the coexisting phases [Lu2018, Su2019b]. The deformation-driven nanoscale refinement observed in such alloys seems to be further promoted by the very small coherent interface energies among the different phases and microstructure ingredients, that is, the FCC phase, the HCP phase, twins and stacking faults. The similarity in phase energy can also lead to a bidirectional TRIP effect, in which FCC-structured matrix portions transform under load into HCP regions and vice versa, depending on the local, micromechanical stresses. This effect leads to an extreme microstructure refinement down to the nanometer regime [Lu2018].

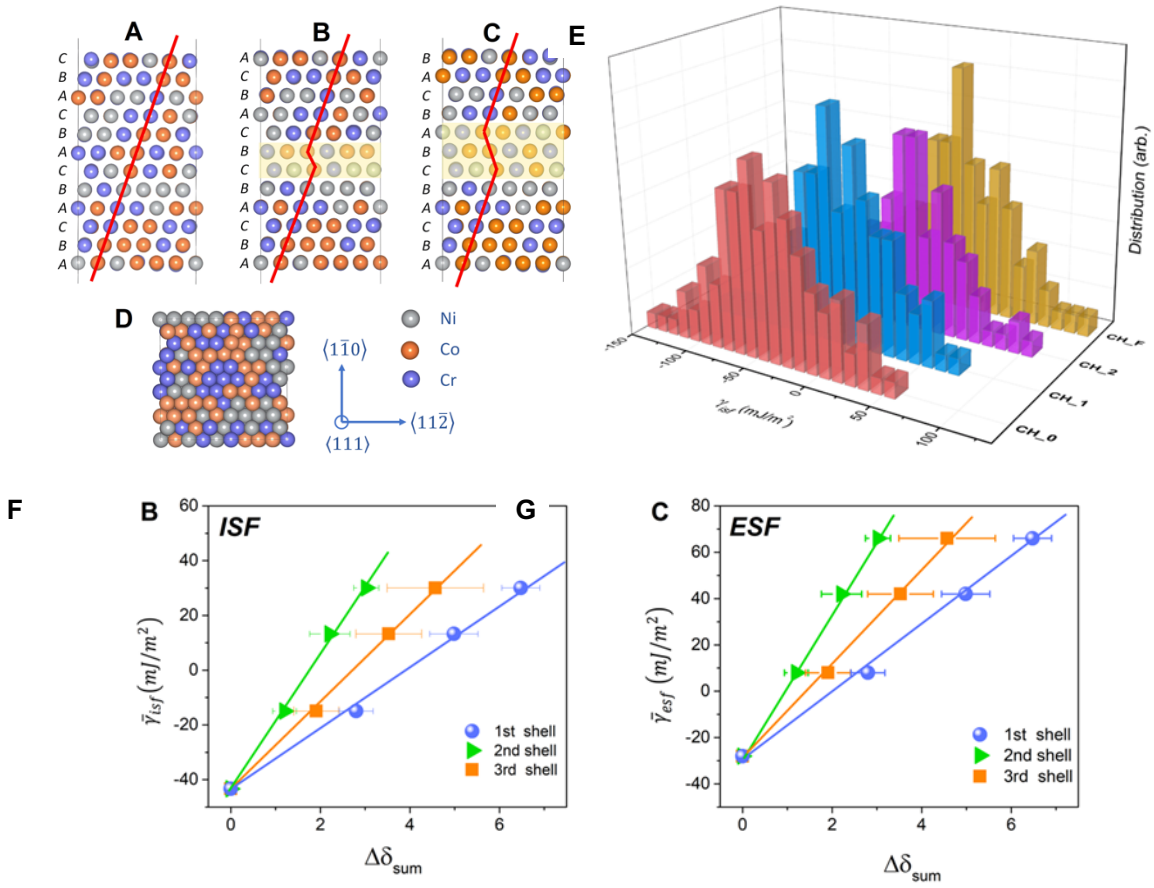

Fig. 6. **Role of local chemical ordering on the stacking fault energy calculated by DFT for solid-solution CrCoNi alloys.** (A-C) show the side view images of atomic configurations in the original fcc structure, with ISF and ESF, respectively; the yellow shade indicates the stacking fault; the plane labels of ABC… represent the sequence of close-packed (111) plane; (D) Top view image showing the close-packed (111) plane. (E) Distribution of intrinsic stacking fault energy, γ_{isf}, for the CrCoNi alloys in four specific states (CH_0, CH_1, CH_2 and CH_F) which span from random solid solution to the highest degree of chemical ordering. Totally 108 stacking faults were considered for analysis in each group. The average energy, $\bar{\gamma}_{isf}$ and $\bar{\gamma}_{esf}$ in (F) and (G), respectively, among those four groups were correlated with the total nonproportional number of local atomic pairs, $\Delta\delta_{sum}$, for the first, second and third nearest-neighbor shells. [Ding2018].

Interesting effects in HEAs may be expected owing to the multi-element co-decoration of lattice defects. Wheras traditional segregation phenomena such as Cottrell atmospheres, grain-boundary segregation and Suzuki decoration are well known, they may work differently when involving many interacting species that co-segregate. The thermodynamic and kinetic competition among the decorating species, as well as their interactions once segregated, may lead to novel structures and phenomena.

Another avenue of interesting research pertains to the role of interstitial elements in HEAs. Several groups studied the influence of C on phase stability, carbide formation and mechanical properties, but other elements such as N, O, H and B are also interesting doping candidates in HEAs. For example, it was recently shown that O, which is normally a rather harmful interstitial element in metals, aids in forming ordered O-Ti-Zr rich clusters in an O-doped TiZrHfNb HEA, enhancing its strength and ductility [Lei2018]. Even the most harmful interstitial element in metallic alloys, H, has been found to lend a certain resistance to hydrogen embrittlement in HEAs. This effect was attributed to the fact that H reduces the material's stacking-fault energy, thus providing higher local strain hardening [Luo2018]. To aid future research efforts, several theoretical and experimental tools need to be improved (Box 3).

In general, we believe that more attention should be placed on potential innovative applications for HEAs. Most efforts in the field are focused on mechanical properties but recent works also revealed unexpected beneficial features of HEAs that might be interesting for magnetic, invar or catalytic applications. Particularly HEAs with multi-functional properties might lead to new processes or products. Thus, it will be worth exploring where specific properties may be expected that are better than those of established material classes, such as steels or aluminum alloys.

In this regard, it is pertinent to note that nature effectively designs structural architectures to create multifunctional materials with unusual combinations of properties that are often difficult to achieve in a single synthetic material; for example, sea shells possess both strength and ductility, which are often mutually exclusive properties in man-made materials [Wegst2015]. HEAs offer the possibility of multi-functionality but without the need for bottom-up (atomic-scale) processing. For example, strain hardening to attain strength and ductility in CoCrNi-based HEAs is promoted not simply through structure but also via composition and the associated mechanism tuning. HEAs with excellent mechanical properties remain to be engineered to achieve other properties, such as corrosion and/or oxidation resistance or resistance to stress-corrosion cracking, for example by alloy additions to change the composition of the protective self-passivating oxides that form on their surface. Understanding and quantifying diffusion in multi-component systems is another area of research that needs to be revived to develop creep-resistant HEAs.

These challenges will undoubtedly provide innumerable promising pursuits for materials

scientists and engineers in the never-ending mission to design and develop superior materials to meet the needs of next-generation engineering applications, particularly for energy and transportation.

Acknowledgments

This study was supported by the U.S. Department of Energy, Office of Science, Office of Basic Energy Sciences, Division of Materials Sciences and Engineering, through the Materials Science and Technology Division at the Oak Ridge National Laboratory (E.P.G.) and the Materials Sciences Division at the Lawrence Berkeley National Laboratory (R.O.R.). D.R. was supported by the European Research Council through the 7th Framework Programme (FP7/2007-2013) ERC Advanced Grant SMARMET (Grant Agreement 290998) and through the German Research Foundation (DFG) through the Priority Programme "Compositionally Complex Alloys – High Entropy Alloys (CCA-HEA)" (SPP 2006).

Author contributions

E.P.G., D.R., and R.O.R. developed the ideas for the paper and wrote the manuscript.

Competing interests

The authors declare no competing interests.

References

Abu-Odeh, A., Galvan, E., Kirk, T., Mao, H., Chen, Q. et al. Efficient exploration of the high entropy alloy composition-phase space. *Acta Mater*. **152**, 41-57 (2018).

Abuzaid, W., & Sehitoglu, H. Critical resolved shear stress for slip and twin nucleation in single crystalline FeNiCoCrMn high entropy alloy. *Mater. Char*. **129**, 288-299 (2017).

Basinski, Z. S., Foxall, R. A., & Pascual, R. Stress equivalence of solution hardening. *Scr. Metall*. **6**, 807-814 (1972).

Bhattacharjee, P. P., Sathiaraj, G.D., Zaid, M., Gatti, J.R., Lee, C. et al. Microstructure and texture evolution during annealing of equiatomic CoCrFeMnNi high-entropy alloy, *J. Alloy. Compd*. **587**, 544-552 (2014).

Bönisch, M., Wu, Y., & Sehitoglu, H. Hardening by slip-twin and twin-twin interactions in FeMnNiCoCr. *Acta Mater*. **153**, 391-403 (2018).

Borkar, T., Gwalani, B., Choudhuri, D., Mikler, C. V., Yannetta, C. J. et al. A combinatorial assessment of Al*x*CrCuFeNi2 ($0 < x < 1.5$) complex concentrated alloys: microstructure, microhardness, and magnetic properties. *Acta Mater*. **116**, 63-76 (2016).

Borkar, T. Chaudhary, V., Gwalani, B., Choudhury, D., Mikler, C. V. et al. A combinatorial approach for assessing the magnetic properties of high entropy alloys: role of Cr in AlCoxCr1-xFeNi. *Adv. Eng. Mater*. **19**, 1700048 (2017).

Bracq, G., Laurent-Brocq, M., Perrière, L., Pirès, R., Joubert, J.-M. et al. The fcc solid solution stability in the Co-Cr-Fe-Mn-Ni multi-component system. *Acta Mater*. **128**, 327-336 (2017).

Butt, M. Z., & Feltham, P. Solid-solution hardening. *Acta Metall*. **26**, 167-173 (1978)

Cantor, B., Chang, I. T. H., Knight, P., & Vincent, A. J. B. Microstructural development in equiatomic multicomponent alloys. *Mater. Sci. Eng. A* **375**, 213-218 (2004).

Cantor, B. *Ann. Chim.-Sci. Mater*. **32** 245 (2007).

Cantor, B., Multicomponent and high entropy alloys. *Entropy* **16**, 4749-4768 (2014).

Chen, H. L., Mao, H. H., & Chen, Q. Database development and CALPHAD calculations for high entropy alloys: challenges, strategies, and tips. *Mater. Chem. Phys*. **210**, 279-290 (2018).

Collins, P. C., Banerjee, R., Banerjee, S., Fraser, H. L. Laser deposition of compositionally graded titanium-vanadium and titanium-molybdenum alloys. *Mater. Sci. Eng. A* **352**, 118-128 (2003).

Couzinié, J. P., Dirras, G., Perrière, L., Chauveau, T. Leroy, E. et al. Microstructure of a near-equimolar refractory high-entropy alloy. *Mater. Lett*. **126**, 285-287 (2014).

Couzinié, J. P., Lilensten, L., Champion,Y., Dirras, G., Perrière, L. et al. On the room temperature deformation mechanisms of a TiZrHfNbTa refractory high-entropy alloy. *Mater. Sci. Eng*. A **645**, 255-263 (2015).

Christian, J.W. & Mahajan, S. Deformation twinning. *Prog. Mater. Sci*. **39**, 1-157 (1995).

Deng, Y., Tasan, C. C., Pradeep, K. G., Springer, H., Kostka, A. et al. Design of a twinning-induced plasticity high entropy alloy. *Acta Mater*. **94**, 124-133 (2015).

Ding, J., Yu, Q., Asta, M., & Ritchie, R. O. Tunable stacking fault energies by tailoring local chemical order in CrCoNi medium-entropy alloys. *Proc. Nat. Acad. Sci*. USA **115**, 8819-8924 (2018).

Dirras, G., Gubicza, J., Heczel, A., Lilensten, L, Couzinié, J. P. et al. Microstructural investigation of plastically deformed Ti20Zr20Hf20Nb20Ta20 high entropy alloy by X-ray diffraction and transmission electron microscopy. *Mater. Char*. **108**, 1-7 (2015).

Dirras, G., Lilensten, L., Djemia, P., Laurent-Brocq, M., Tingaud, D. et al. Elastic and plastic properties of as-cast equimolar TiHfZrTaNb high-entropy alloy. *Mater. Sci. Eng. A* **654**, 30-38 (2016).

Dobbelstein, H., Gurevich, E. L., George, E. P., Ostendorf, A., & Laplanche G. Laser metal deposition of compositionally graded TiZrNbTa refractory high-entropy alloys using elemental powder blends. *Additive Manufacturing* **25**, 252-262 (2019).

Friedel, J. Dislocations. Oxford: Pergamon Press, 1965.

Feuerbacher, M., Heidelmann, M., & Thomas, C., Hexagonal high-entropy alloys. *Mater. Res. Lett*. **3**, 1-6 (2015).

Gali, A. & George, E. P. Tensile properties of high- and medium-entropy alloys. *Intermetallics* **39**, 74-78 (2013).

Gao, M. C., Zhang, C, Gao, P., Zhang, F., Ouyang, L. Z. et al. Thermodynamics of concentrated solid solution alloys. *Curr. Opinion Sol. State Mater. Sci*. **21**, 238-251 (2017).

Gludovatz, B., Hohenwarter, A., Catoor, D., Chang, E. H., George, E.P. et al. A fracture-resistant high-entropy alloy for cryogenic applications. *Science* **345**, 1153–1158 (2014).

Gludovatz, B., Hohenwarter, A., Thurston, K. V. S., Bei. H., Wu, Z. et al. Exceptional damage-tolerance of a medium-entropy alloy CrCoNi at cryogenic temperatures. *Nat. Commun*. **7**, 10602 (2016).

Gorsse, S., & Tancret, F. Current and emerging practices of CALPHAD toward the development of high entropy alloys and complex concentrated alloys. *J. Mater. Res*. **33**, 2899-2923 (2018a).

Gorsse, S., & Senkov, O. N., About the reliability of CALPHAD predictions in multicomponent systems. *Entropy* **20**, 899 (2018b).

Gutierrez-Urrutia, I., & Raabe, D. Multistage strain hardening through dislocation substructure and twinning in a high strength and ductile weight-reduced Fe-Mn-Al-C steel. *Acta Mater*. **60**, 5791-5802 (2012).

Haas, S., Mosbacher, M., Senkov, O. N., Feuerbacher, M., Freudenberger, J. et al. Entropy determination of single-phase high entropy alloys with different crystal structures over a wide temperature range. *Entropy* **20**, 654 (2018).

Haasen, P. Plastic deformation of nickel single crystals at low temperatures. *Philos. Mag*. **3**, 384-418 (1958).

Haglund, A., Koehler, M., Catoor, D., George, E. P., & Keppens, V. Polycrystalline elastic moduli of a high-entropy alloy at cryogenic temperatures. *Intermetallics* **58**, 62-64 (2015).

Hanak, J. J. The “multiple-sample concept” in materials research: synthesis, compositional analysis, and testing of entire multicomponent systems. *J. Mater. Sci*. **5**, 964-971 (1970).

He, J. Y., Zhu, C., Zhou, D. Q., Liu, W. H., Nieh, T. G. et al. Steady state flow of the FeCoNiCrMn high entropy alloy at elevated temperatures. *Intermetallics* **55**, 9-14 (2014).

Holdren, J. P. Materials genome initiative for global competitiveness. Washington, DC: National Science and Technology Council (2011).

Huang, P. K., Yeh, J. W., Shun, T. T., & Chen. S. K. Multi-principal-element alloys with improved oxidation and wear resistance for thermal spray coating. *Adv. Eng. Mater*. **6**, 74-78 (2004).

Huang, S., Li, W., Lu, S., Tian, F., Shen, J. et al. Temperature dependent stacking fault energy of FeCrCoNiMn high entropy alloy. *Scr. Mater*. **108**, 44-47 (2015).

Huang, H. L., Wu, Y., He, J. Y., Wang, H, Liu, X. J., et al. Phase-transformation ductilization of brittle high-entropy alloys via metastability engineering. *Adv. Mater*. **29**, 1701678 (2017).

Jo, Y. H., Jung, S., Choi, W. M., Sohn, S. S., Kim, H. S. et al. Cryogenic strength improvement by utilizing room-temperature deformation twinning in a partially recrystallized VCrMnFeCoNi high-entropy alloy. *Nat. Commun*. **8**, 15719 (2017).

Juan, C. C., Tsai, M. H., Tsai, C. W., Lin, C. M., Wang, W. R. et al. Enhanced mechanical properties of HfMoTaTiZr and HfMoNbTaTiZr refractory high-entropy alloys. *Intermetallics* **62**, 76-83 (2015).

Juan, C-C., Tsai, M-H., Tsai, C-W., Hsu, W-L., Lin, C-M. et al. Simultaneously increasing the strength and ductility of a refractory high-entropy alloy via grain refining. *Mater. Lett*. **184**, 200-203 (2016).

Kauffmann, A., Stüber, M., Leiste, H., Ulrich, S., Schlabach, S. et al. Combinatorial exploration of the high entropy alloy system Co-Cr-Fe-Mn-Ni. *Surf. Coating Tech*. **325**, 174-180 (2017).

Kennedy, K., Stefansky, T., Dvy, G., Zackay, V. F., & Parker, E. R., Rapid method for determining ternary-alloy phase diagrams. *J. Appl. Phys*. **36**, 3808-3810 (1965).

King, D. J. M., Middleburgh, S. C., McGregor, A. G., & Cortie, M. B. Predicting the formation and stability of single phase high-entropy alloys. *Acta Mater*. **104**, 172-179 (2016).

Kireeva, I. V., Chumlyakov, Yu. I., Pobedennaya, Z. V., Kuksgausen, I. V., & Karaman, I. Orientation dependence of twinning in single crystalline CoCrFeMnNi high-entropy alloy. *Mater. Sci. Eng. A* **707**, 176-181 (2017).

Kireeva, I. V., Chumlyakov, Yu. I., Pobedennaya, Z. V., Vyrodova, A. V., & Karaman, I. Twinning in [001]-oriented single crystals of CoCrFeMnNi high-entropy alloy at tensile deformation. *Mater. Sci. Eng. A* **713**, 253-259 (2018).

Knoll, H., Ocylok, S., Weisheit, A., Springer, H., Jägle, E. et al. Combinatorial alloy design by laser additive manufacturing. *Steel Res. Int*. **88**, 1600416 (2017).

Koppenaal, T. J., & Fine, M. E. Solid solution strengthening in alpha Cu-Al single crystals. *Trans. Metall. Soc. AIME* **224**, 347-353 (1962).

Kozelj, K., Vrtnik, V., Jelen, A., Jazbec, S., Jaglicic, Z. et al. Discovery of a superconducting high-entropy alloy. *Phys. Rev. Lett*. **113**, 107001 (2014).

Laplanche, G., Gadaud, P., Horst, O., Otto, F., Eggeler, G. et al. Temperature dependencies of the elastic moduli and thermal expansion coefficient of an equiatomic, single-phase CoCrFeMnNi high-entropy alloy. *J. Alloys Cmpd*. **623**, 348-353 (2015a).

Laplanche, G., Horst, O., Otto, F., Eggeler, G., George, E. P. Microstructural evolution of a CoCrFeMnNi high-entropy alloy after swaging and annealing. *J. Alloys Cmpd*. **647**, 548-557 (2015b).

Laplanche, G., Kostka, A., Horst, O. M., Eggeler, G., & George, E. P. Microstructure evolution and critical stress for twinning in the CrMnFeCoNi high-entropy alloy. *Acta Mater*. **118**, 152-163 (2016).

Laplanche, G., Kostka, A., Reinhart, C., Hunfeld, J., Eggeler, G. et al. Reasons for the superior mechanical properties of medium-entropy CrCoNi compared to high-entropy CrMnFeCoNi. *Acta Mater*. **128**, 292-303 (2017).

Laplanche, G., Bonneville, J., Varvenne, C., Curtin, W. A., & George, E. P. Thermal activation parameters of plastic flow reveal deformation mechanisms in the CrMnFeCoNi high-entropy alloy. *Acta Mater*. **143**, 257-264 (2018a).

Laplanche, G., Berglund, S., Reinhart, C., Kostka, A., Fox, F. et al. Phase stability and kinetics of σ-phase precipitation in CrMnFeCoNi high-entropy alloys. *Acta Mater*. **161**, 338-351 (2018b).

Laurent-Brocq, M., Akhatova, A., Perrière, L., Chebini, S., Sauvage, X. et al. Insights into the phase diagram of the CrMnFeCoNi high entropy alloy. *Acta Mater*. **88**, 355-365 (2015).

Lei, Z., Liu, X., Wu, Y., Wang, H., Jiang, S. et al. Enhanced strength and ductility in a high-entropy alloy via ordered oxygen complexes. *Nature* **563**, 546-550 (2018).

Li, Z., Pradeep, K. G., Deng, Y., Raabe, D., & Tasan, C. C. Metastable high-entropy dual-phase alloys overcome the strength-ductility trade-off. *Nature* **534**, 227-230 (2016).

Li, Z., & Raabe, D. Strong and ductile non-equiatomic high-entropy alloys: design, processing, microstructure, and mechanical properties. *JOM* **69**, 2099-2106 (2017a).

Li, Z., Körmann, F., Grabowski, B., Neugebauer, J., & Raabe, D. Ab initio assisted design of quinary dual-phase high-entropy alloys with transformation-induced plasticity. *Acta Mater*. **136**, 262-270 (2017b).

Li, Z., Tasan, C. C., Springer, H., Gault, B., & Raabe, D. Interstitial atoms enable joint twinning and transformation induced plasticity in strong and ductile high-entropy alloys. *Sci. Reports* **7**, 40704 (2017c).

Li, Z., Tasan, C. C., Pradeep, K. G., & Raabe, D. A TRIP-assisted dual-phase high-entropy alloy: grain size and phase fraction effects on deformation behavior. *Acta Mater*. **131**, 323-335 (2017d).

Li, Z., & Raabe, D. Influence of compositional inhomogeneity on mechanical behavior of an interstitial dual-phase high-entropy alloy. *Mater. Chem. Phys*. **210**, 29-36 (2018a).

Li, Z., Ludwig, A., Savan, A., Springer, H., & Raabe, D. Combinatorial metallurgical synthesis and processing of high-entropy alloys. *J. Mater. Res*. **33**, 3156-3169 (2018b).

Li, Y. J., Kostka, A., Savan A., Stein, H. S., & Ludwig, A. Accelerated atomic-scale exploration of phase evolution in compositionally complex materials. *Mater. Horizons* **5**, 86-92 (2018c).

Li, Y. J., Kostka, A., Savan A., & Ludwig, A. Atomic-scale investigation of fast oxidation kinetics of nanocrystalline CrMnFeCoNi alloy thin films. *J. Alloys Cmpd*. **766**, 1080-1085 (2018d).

Lilensten, L., Couzinié, J. P., Perrière, L., Bourgon, J., Emery, N. et al. New structure in refractory high-entropy alloys. *Mater. Lett*. **132**, 123-125 (2014).

Lilensten, L., Couzinié, J. P., Bourgon, J., Perrière, L., Dirras, G. et al. Design and tensile properties of a bcc Ti-rich high-entropy alloy with transformation-induced plasticity. *Mater. Res. Lett*. **5**, 110-116 (2017).

Lin, C-M., Juan, C-C., Chang, C-H., Tsai, C-W., Yeh, J-W. Effect of Al addition on mechanical properties and microstructure of refractory AlxHfNbTaTiZr alloys. *J. Alloys Cmpd*. **624**, 100-107 (2015).

Liu, W.H., Wu, Y., He, J. Y., Nieh, T. G., Lu, Z. P. Grain growth and the Hall-Petch relationship in a high-entropy FeCrNiCoMn alloy. *Scr. Mater*. **68**, 526-529 (2013).

Liu, W. H., Lu, Z. P., He, J. Y., Luan, J. H., Wang, Z. J. et al. Ductile $CoCrFeNiMo_x$ high entropy alloys strengthened by hard intermetallic phases. *Acta Mater*. **116**, 332-342 (2016).

Ludwig, A., Zarnetta, R., Hamann, S., Savan, A. & Thienhaus, S. Development of multifunctional thin films using high-throughput experimentation methods. *Int. J. Mater. Res*. **99**, 1144-1149 (2008).

Lu, W., Liebscher, C.H., Dehm, G., Raabe, D., & Li, Z. Bidirectional transformation enables hierarchical nanolaminate dual-phase high-entropy alloys. *Adv. Mater.* **30**, 1804727 (2018).

Luo, H., Li, Z., & Raabe, D. Hydrogen enhances strength and ductility of an equiatomic high-entropy alloy. *Sci. Reports* **7**, 9892 (2017).

Luo, H., Lu, W., Fang, X., Ponge, D., Li, Z., & Raabe, D. Beating hydrogen with its own weapon: Nano-twin gradients enhance embrittlement resistance of a high-entropy alloy. *Materials Today* **21**, 1003-1009 (2018).

Ma, D., Grabowski, B., Körmann, F., Neugebauer, J., & Raabe. D. Ab initio thermodynamics of the CoCrFeMnNi high entropy alloy: importance of entropy contributions beyond the configurational one. *Acta Mater*. **100**, 90-97 (2015a).

Ma, D., Yao, M., Pradeep, K. G., Tasan, C. C., Springer, H. et al. Phase stability of non-equiatomic CoCrFeMnNi high entropy alloys. *Acta Mater*. **98**, 288-296 (2015b).

Mahajan, S. Twin-slip and twin-twin interactions in Mo-35 at.% Re alloy. *Philos. Mag*. **23**, 781-794 (1971).

Mahajan, S., & Chin, G. Y. Formation of deformation twins in FCC crystals. *Acta Metall*. **21**, 1353-1363 (1973).

Mao, H. H., Chen, H. L., & Chen, Q. TCHEA1: a thermodynamic database not limited for "high entropy" alloys. *J. Phase Equil. Diff*. **38**, 353-368 (2017).

Mertens, R., Sun, Z. M., Music, D., & Schneider, J. M. Effect of the composition on the structure of Cr-Al-C investigated by combinatorial thin film synthesis and ab initio calculations. *Adv. Eng. Mater*. **6**, 903-907 (2004).

Meyers, M. A., Vöhringer, O., Lubarda, V. A. The onset of twinning in metals: a constitutive description. *Acta Mater*. **49**, 4025-4039 (2001).

Miracle, D. B., & Senkov, O. N. A critical review of high entropy alloys and related concepts. *Acta Mater*. **122**, 448-511 (2017).

Nene, S.S., Liu, K., Frank, M., Mishra, R.S., Brennan, R.E. et al. Enhanced strength and ductility in a friction stir processing engineered dual phase high entropy alloy. *Sci. Reports* **7**, 16167 (2017).

Okamoto, N. L., Fujimoto, S., Kambara, Y., Kawamura, M., Chen, Z. M. T. et al. Size effect, critical resolved shear stress, stacking fault energy, and solid solution strengthening in the CrMnFeCoNi high-entropy alloy. *Sci. Reports* **6**, 35863 (2016a).

Okamoto, N. L., Yuge, K., Tanaka, K., Inui, H., & George, E. P. Atomic displacement in the CrMnFeCoNi high-entropy alloy – a scaling factor to predict solid solution strengthening. *AIP Advances* **6**, 125008 (2016b).

Otto, F., Yang, Y., Bei, H., & George, E. P. Relative effects of enthalpy and entropy on the phase stability of equiatomic high-entropy alloys. *Acta Mater*. **61**, 2628-2638 (2013a).

Otto, F., Dlouhy, A., Somsen, Ch., Bei, H., Eggeler, G. et al. The influences of temperature and microstructure on the tensile properties of a CoCrFeMnNi high-entropy alloy. *Acta Mater*. **61**, 5743-5755 (2013b).

Otto, F., Hanold, N. L., & George, E. P. Microstructural evolution after thermomechanical processing in an equiatomic single-phase CoCrFeMnNi high-entropy alloy with special focus on twin boundaries. *Intermetallics* **54**, 39-48 (2014).

Otto, F., Dlouhy, A., Pradeep, K. G., Kubenova, M., Raabe, D. et al. Decomposition of the single-phase high-entropy alloy CrMnFeCoNi after prolonged anneals at intermediate temperatures. *Acta Mater*. **112**, 40-52 (2016).

Patriarca, L, Ojha, A., Sehitoglu, H., & Chumlyakov, Y. I., Slip nucleation in single crystal FeNiCoCrMn high entropy alloy. *Scr. Mater*. **112**, 54-57 (2016).

Pickering, E. J., Munoz-Moreno, R., Stone, H. J., & Jones, N. G. Precipitation in the equiatomic high-entropy alloy CrMnFeCoNi. *Scripta Mater*. **113**, 106-109 (2016a).

Pickering, E. J., & Jones, N. G. High-entropy alloys: a critical assessment of their founding principles and future prospects. *Int. Mater. Rev*. **61**, 183-202 (2016b).

Poletti, M. G., & Battezzati, L. Electronic and thermodynamic criteria for the occurrence of high-entropy alloys in metallics systems. *Acta Mater*. **75**, 297-306 (2014).

Pradeep, K. G., Tasan, C. C., Yao, M. J., Deng, Y., Springer, H. et al. Non-equiatomic high entropy alloys: approach towards rapid alloy screening and property-oriented design *Mater. Sci. Eng. A* **648**,183-192 (2015).

Qiao, J. W., Bao, M. L., Zhao, Y. J., Yang, H. J., Wu, Y. C. et al. Rare-earth high entropy alloys with hexagonal close-packed structure. *J. Appl. Phys*. **124**, 195101 (2018).

Raabe, D., Springer, H., Gutierrez-Urrutia, I., Roters, F., Bausch, M. et al. Alloy design, combinatorial synthesis, and microstructure–property relations for low-density Fe-Mn-Al-C austenitic steels. *JOM*, **66**, 1845-1856 (2014).

Raabe, D., Tasan, C.C., Springer, H., & Bausch, M. From high-entropy alloys to high-entropy steels. *Steel Res. Int*. **86**, 1127-1138 (2015).

Raabe, D., Roters, F., Neugebauer, J., Gutierrez-Urrutia, I., Hickel, T. et al. Ab initio-guided design of twinning-induced plasticity steels. *MRS Bull*. **41**, 320-325 (2016).

Rar, A., Frafjord, J. J., Fowlkes, J. D., Specht, E. D., Rack, P. D. et al. PVD synthesis and high-throughput property characterization of Ni-Fe-Cr alloy libraries. *Meas. Sci. Technol. A* **16**, 46-53 (2005).

Salishchev, G. A., Tikhonovsky, M. A., Shaysultanov, D. G., Stepanov, N. D., Kuznetsov, A. V. et al. Effect of Mn and V on structure and mechanical properties of high-entropy alloys based on CoCrFeNi system, *J. Alloy. Compd*. **591**, 11-21 (2014).

Schön, C. G., Duong, T., Wang, Y. & Arróyave, R. Probing the entropy hypothesis in highly concentrated alloys. *Acta Mater*. **148**, 263-279 (2018).

Schuh, B., Mendez-Martin, F., Völker, B., George, E. P., Clemens, H. et al. Mechanical properties, microstructure and thermal stability of a nanocrystalline CoCrFeMnNi high-entropy alloy after severe plastic deformation. *Acta Mater*. **96**, 258-268 (2015).

Schuh, B., Volker, B., Todt, J., Schell, N., Perrière, L. et al. Thermodynamic instability of a nanocrystalline, single-phase TiZrNbHfTa alloy and its impact on the mechanical properties. *Acta Mater*. **142**, 201-212 (2018).

Senkov, O.N., Wilks, G.B., Miracle, D. B., Chuang, C.P., & Liaw, P. K., Refractory high-entropy alloys. *Intermetallics* **18**, 1758-1765 (2010).

Senkov, O. N., & Woodward, C. F., Microstructure and properties of a refractory NbCrMo0.5Ta0.5TiZr alloy. *Mater. Sci. Eng*. A **529**, 311-320 (2011a).

Senkov, O. N., Wilks, G. B., Scott, J. M., & Miracle, D. B. Mechanical properties of Nb25Mo25Ta25W25 and V20Nb20Mo20Ta20W20 refractory high entropy alloys. *Intermetallics* **19**, 698-706 (2011b).

Senkov, O.N., Scott, J.M., Senkova, S.V., Miracle, D.B., & Woodward, C.F. Microstructure and room temperature properties of a high-entropy TaNbHfZrTi alloy. *J. Alloys Cmpd*. **509**, 6043-6048 (2011c).

Senkov, O. N., Scott, J. M., Senkova, S. V., Meisenkothen, F., Miracle, D.B., et al. Microstructure and elevated temperature properties of a refractory TaNbHfZrTi alloy. *J. Mater. Sci*. **47**, 4062-4074 (2012).

Senkov, O. N., Senkova, S. V., & Woodward, C. Effect of aluminum on the microstructure and properties of two refractory high-entropy alloys. *Acta Mater*. **68**, 214-228 (2014).

Senkov, O.N., & Semiatin, S.L. Microstructure and properties of a refractory high-entropy alloy after cold working. *J. Alloys Cmpd*. **649**, 1110-1123 (2015).

Sheikh, S., Shafeie, S., Hu, Q., Ahlström, J., Persson, C. et al. Alloy design for intrinsically ductile refractory high-entropy alloys. *J. Appl. Phys*. **120**, 164902 (2016).

Shun, T. T., Hung, C. H., & Lee, C. F. Formation of ordered/disordered nanoparticles in FCC high entropy alloys. *J. Alloys Compd*. **493**, 105-109 (2010).

Singh, S., Wanderka, N., Murty, B. S., Glatzel, U., & Banhart, J. Decomposition in multi-component AlCoCrCuFeNi high-entropy alloy. *Acta Mater*. **59**, 182-190 (2011).

Slone, C. E., Miao, J. George, E. P., & Mills, M. J. Achieving ultra-high strength and ductility in equiatomic CrCoNi with partially recrystallized microstructures. *Acta Mater*. **165**, 497-507 (2019).

Smith, T. M., Hooshmand, M. S., Esser, B. D., Otto, F., McComb, D. W. et al. Atomic-scale characterization and modeling of 60° dislocations in a high-entropy alloy. *Acta Mater*. **110**, 352-362 (2016).

Sohn, S.S., Kwiatkowski da Silva, A., Ikeda, Y., Körmann, F. et al. Ultrastrong medium-entropy single-phase alloys designed via severe lattice distortion. *Adv. Mater*. in press (2019).

Song, H., Tian, F., & Wang D. Thermodynamic properties of refractory high entropy alloys. *J. Alloys Cmpd*. **682**, 773-777 (2016).

Soler, R., Evirgen, A., Yao, M., Kirchlechner, C., Stein, F. et al. Microstructural and mechanical characterization of an equiatomic YGdTbDyHo high entropy alloy with hexagonal close-packed structure. *Acta Mater*. **156**, 86-96 (2018).

Specht, E. D., Rar, A., Pharr, G. M., George, E. P., Zschack, P. et al. Rapid structural and chemical characterization of ternary phase diagrams using synchrotron radiation. *J. Mater. Res*. **18**, 2522-2527 (2003)

Springer, H., & Raabe, D. Rapid alloy prototyping: compositional and thermo-mechanical high throughput bulk combinatorial design of structural materials based on the example of 30Mn–1.2 C–xAl triplex steels, *Acta Mater*. **60**, 4950-4959 (2012).

Steinmetz, D. R., Jäpel, T., Wietbrock, B., Eisenlohr, P., Gutierrez-Urrutia, I. et al. Revealing the strain-hardening behavior of twinning-induced plasticity steels: theory, simulations, experiments. *Acta Mater*. **6**, 494-510 (2013).

Stepanov, N. D., Shaysultanov, D. G., Yurchenko, N. Y., Zherebtsov, S. V., Ladygin, A. N. et al. High temperature deformation behavior and dynamic recrystallization in CoCrFeMnNi high entropy alloy, *Mater. Sci. Eng. A* **636**, 188-195 (2015).

Stepanov, N., Tikhonovsky, M., Yurchenko, N., Zyabkin, D., Klimova, M. et al. Effect of cryo-deformation on structure and properties of CoCrFeNiMn high-entropy alloy. *Intermetallics* **59**, 8-17 (2015).

Stepanov, N. D., Yurchenko, N. Yu., Zherebtsov, S. V., Tikhonovsky, M. A., & Salishchev, G. A. Aging behavior of the HfNbTaTiZr high entropy alloy. *Mater. Lett*. **211**, 87-90 (2018).

Takeuchi, A., Amiya, K., Wada, T., Yubuta, K., & Zhang, W. High-entropy alloys with a hexagonal close-packed structure designed by equi-atomic alloy strategy and binary phase diagrams, *JOM* **66**, 1984-1992 (2014).

Su, J., Raabe, D., & Li, Z., Hierarchical microstructure design to tune the mechanical behavior of an interstitial TRIP-TWIP high-entropy alloy. *Acta Mater*. **163**, 40-54 (2019).

Su, J., Wu., X., Raabe, D., & Li, Z., Deformation-driven bidirectional transformation promotes bulk nanostructure formation in a metastable interstitial high entropy alloy. *Acta Mater*. in press (2019b).

Tasan, C. C., Deng, Y., Pradeep, K. G., Yao, M. J., Springer, H. et al. Composition dependence of phase stability, deformation mechanisms, and mechanical properties of the CoCrFeMnNi high-entropy alloy system. *JOM* **66**, 1993-2001 (2014).

Tian, F., Delczeg, L., Chen, N., Varga, K. L., Shen, J. et al. Structural stability of NiCoFeCrAl high-entropy alloy from ab initio theory. *Phys. Rev. B* **88**, 085128 (2013).

Tong, C. J., Chen, Y. L., Chen, S. K., Yeh, J. W., Shun, T.T. et al. Microstructure characterization of AlxCoCrCuFeNi high-entropy alloy system with multi-principal elements. *Metall. Mater. Trans. A* **36**, 881-893 (2005).

Tracy, C. L., Park, S., Rittman, D. R., Zinkle, S. J., Bei, H. et al. High-pressure synthesis of a hexagonal close-packed phase of the high-entropy alloy CrMnFeCoNi. *Nat. Commun*. **8**, 15634 (2017).

Traub, H. Neuhäuser, H. Schwink, Ch. Investigations of yield region of concentrated Cu-Ge and Cu-Zn single crystals. 1. Critical resolved shear-stress, slip line formation and true strain rate. *Acta Metall*. **25**, 437-446 (1977).

Troparevsky, M. C., Morris, J. R., Kent, P. R. C., Lupini, A. R., & Stocks, G. M. Criteria for predicting the formation of single-phase high-entropy alloys. *Phys. Rev. X* **5**, 011041 (2015).

Troparevsky, M. C., Morris, J. R., Daene, M., Wang, Y. Lupini, A. R. et al. Beyond atomic sizes and Hume-Rothery rules: understanding and predicting high-entropy alloys. *JOM* **67**, 2350-2363 (2015b).

Tsai, K. Y., Tsai, M. H., & Yeh, J. W., Sluggish diffusion in Co–Cr–Fe–Mn–Ni high-entropy alloys. *Acta Mater*. **61**, 4887-4897 (2013).

Tsai, M. H., & Yeh, J. W. High-entropy alloys: a critical review. *Mater. Res. Lett*. **2**, 107-123 (2014).

van de Walle, A., & Asta, M. Self-driven lattice-model Monte Carlo simulations of alloy thermodynamic properties and phase diagrams. *Modelling Simul. Mater. Sci. Eng*. **10**, 521-538 (2002).

Varvenne, C., Aitor, L., & Curtin, W. A. Theory of strengthening in fcc high entropy alloys. *Acta Mater*. **118**, 164-176 (2016).

Varvenne, C., Leyson, G. P. M., Ghazisaeidi, M., & Curtin, W. A. Solute strengthening in random alloys. *Acta Mater*. **124**, 660-683 (2017).

Venables, J. A. Deformation twinning. New York: Gordon & Breach, 1964.

Vrtnik, S., Kozelj, P., Meden, A., Maiti, S., Steurer, W. et al. Superconductivity in thermally annealed Ta-Nb-Hf-Zr-Ti high-entropy alloys. *J. Alloys Cmpd*. **695**, 3530-3540 (2017).

Wang, F. J., & Zhang, Y. Effect of Co addition on crystal structure and mechanical properties of Ti0.5CrFeNiAlCo high entropy alloy. *Mater. Sci. Eng. A* **496**, 214-216 (2008).

Wang, M. Li, Z., & Raabe, D. In-situ SEM observation of phase transformation and twinning mechanisms in an interstitial high-entropy alloy. *Acta Mater*. **147**, 236-246 (2018).

Wegst, U. G. K., Bai, H., Saiz, E., Tomsia A. P., & Ritchie, R. O. Bioinspired structural materials, *Nature Mater*. **14**, 23-36 (2015).

Wille, Th., & Schwink, Ch. Precision measurements of critical resolved shear-stress in CuMn alloys. *Acta Metall*. **34**, 1059-1069 (1986).

Wille, Th., Gieseke, W., & Schwink, Ch. Quantitative analysis of solution hardening in selected copper alloys. *Acta Metall*. **35**, 2679-2693 (1987).

Wilson, P., Field, R., & Kaufman, M. The use of diffusion multiples to examine the compositional dependence of phase stability and hardness of the Co–Cr–Fe–Mn–Ni high entropy alloy system. *Intermetallics* **75**, 15-24 (2016).

Wong, S. L., Madivala, M., Prahl, U., Roters, F. & Raabe, D. A crystal plasticity model for twinning- and transformation-induced plasticity. *Acta Mater.* **118**, 140-151(2016).

Wu, Y., Bönisch, M., Alkan, S., Abuzaid, W., Sehitoglu, H. Experimental determination of latent hardening coefficients in FeMnNiCoCr. *Int. J. Plasticity* **105**, 239-260 (2018).

Wu, Z., Bei, H., Pharr, G. M., & George, E. P. Temperature dependence of the mechanical properties of equiatomic solid solution alloys with face-centered cubic crystal structures. *Acta Mater*. **81**, 428-441 (2014).

Wu, Z., Parish, C. M., & Bei, H., Nano-twin mediated plasticity in carbon-containing FeNiCoCrMn high entropy alloys. *J. Alloys Cmpd*. **647**, 815–822 (2015).

Xiang, X.-D., Sun, X., Briceño, G., Lou, Y., Wang, K.-A. et al. A combinatorial approach to materials discovery. *Science* **268**, 1738-1740 (1995).

Yang, M., Yan, D., Yuan, F., Jiang, P., Ma, E. et al. Dynamically reinforced heterogeneous grain structure prolongs ductility in a medium-entropy alloy with gigapascal yield strength. *Proc. Nat. Acad. Sci*. USA **115**, 7224-7229 (2018).

Yao, M. J., Pradeep, K. G., Tasan, C. C., & Raabe, D. A novel, single phase, non-equiatomic FeMnNiCoCr high-entropy alloy with exceptional phase stability and tensile ductility *Scripta Mater*. **72-73**, 5-8 (2014).

Yardley, V. Povstugar, V., Choi, P. P., Raabe, D., Parsa, A. B. et al. On local phase equilibria and appearance of nanoparticles in the microstructure of single-crystal Ni-base superalloys. *Adv. Eng. Mater*. **18**, 1556-1567 (2016).

Yeh, J. W., Chen, S. K., Lin, S. J., Gan, J. Y., Chin T. S. et al. Nanostructured high-entropy alloys with multiple principal elements: novel alloy design concepts and outcomes. *Adv. Eng. Mater*. **6**, 299-303 (2004).

Yeh, J. W. Recent progress in high-entropy alloys. *Ann. Chim.-Sci. Mater*. **31**, 633-648 (2006).

Yeh, J. W. Alloy design strategies and future trends in high-entropy alloys. *JOM* **65**, 1759-1771 (2013).

Zaddach, A. J., Niu, C., Koch, C. C., & Irving, D. L. Mechanical properties and stacking fault energies of NiFeCrCoMn high-entropy alloy. *JOM* **65**, 1780-1789 (2013).

Zhang, C., Zhang, F., Chen, S., & Cao, W. Computational thermodynamics aided high-entropy alloy design. *JOM* **64**, 839-845 (2012).

Zhang, F., Zhang, C., Chen, C. L., Zhu, J., Cao, W. S. et al. An understanding of high entropy alloys from phase diagram caluculations, *CALPHAD - Computer Coupling of Phase Diagrams and Thermochemistry*. **45**, 1-10 (2014).

Zhang F. X., Zhao, S., Jin, K., Xue, H., Velisa, G., Bei, et al. Local structure and short-range order in a NiCoCr solid solution alloy. *Phys. Rev. Lett.* **118,** 205501 (2017a).

Zhang, F., Wu, Y., Lu, H. B., Zeng, Z. D., Prakapenka, V. B. et al. Polymorphism in a high-entropy alloy. *Nat. Commun*. **8**, 15687 (2017b).

Zhang, Y., Zuo, T. T., Tang, Z., Gao, M. C., Dahmen, K. A. et al. Microstructures and properties of high-entropy alloys. *Prog. Mater. Sci*. **61**, 1-93 (2014).

Zhang, Z. J., Mao, M. M., Wang, J., Gludovatz, B., Zhang, Z. et al. Nanoscale origins of the damage tolerance of the high-entropy alloy CrMnFeCoNi. *Nat. Commun.* **6**, 10143 (2015).

Zhang, Z. J., Sheng, H. W., Wang, Z. J., Gludovatz, B., Zhang, Z. et al. Dislocation mechanisms and 3D twin architectures generate exceptional strength-ductility-toughness combination in CrCoNi medium-entropy alloy. *Nat. Commun.* **8**, 14390 (2017).

Zhao, J.-C., Zheng, X., & Cahill, D.G. High-throughput diffusion multiples. *Mater. Today* **8**, 28-37 (2005).

Zhao, J.-C. Combinatorial approaches as effective tools in the study of phase diagrams and composition–structure–property relationships. *Prog. Mater. Sci*. **51**, 557-631 (2006).

Zhao, Y. L., Yang, T., Tong, Y., Wang, J., Luan, J. H. et al. Heterogeneous precipitation behavior and stacking-fault-mediated deformation in a CoCrNi-based medium-entropy alloy. *Acta Mater*. **138**, 72-82 (2017).

Zhao, Y. J., Qiao, J. W., Ma, S. G., Gao, M. C., Yang, H. J. et al. A hexagonal close-packed high-entropy alloy: the effect of entropy. *Mater. Des*. **96**, 10-15 (2016).

Zhou, Y. J., Zhang, Y., Wang, Y. L., & Chen, G. L. Solid solution alloys of AlCoCrFeNiTix with excellent room-temperature mechanical properties. *Appl. Phys. Lett*. **90**, 181904 (2007).